



**HAL**  
open science

# Rheological Characterization of High Molecular Weight PEO-An Extensive Parametric Experimental Study

Hafiz Ahmad, M'hamed Boutaous, Shihe Xin, Hervé Pabiou, Dennis A Siginer

► **To cite this version:**

Hafiz Ahmad, M'hamed Boutaous, Shihe Xin, Hervé Pabiou, Dennis A Siginer. Rheological Characterization of High Molecular Weight PEO-An Extensive Parametric Experimental Study. *Journal of Fluids Engineering*, 2023, 145 (2), pp.021204. 10.1115/1.4056160 . hal-03859954

**HAL Id: hal-03859954**

**<https://hal.science/hal-03859954>**

Submitted on 18 Nov 2022

**HAL** is a multi-disciplinary open access archive for the deposit and dissemination of scientific research documents, whether they are published or not. The documents may come from teaching and research institutions in France or abroad, or from public or private research centers.

L'archive ouverte pluridisciplinaire **HAL**, est destinée au dépôt et à la diffusion de documents scientifiques de niveau recherche, publiés ou non, émanant des établissements d'enseignement et de recherche français ou étrangers, des laboratoires publics ou privés.

# Rheological Characterisation of High Molecular Weight PEO-An Extensive Parametric Experimental study

Hafiz Ahmad<sup>1,2</sup>, M'hamed Boutaous<sup>1</sup>, Shihe Xin<sup>1</sup>, Hervé Pabiou<sup>1</sup>, Dennis A. Siginer<sup>3</sup>

<sup>1</sup>Univ Lyon, CNRS, INSA-Lyon, Université Claude Bernard Lyon 1, CETHIL  
UMR5008, F-69621, Villeurbanne, France

Email: mhamed.boutaous@insa-lyon.fr, hafiz.ahmad@insa-lyon.fr, shihe.xin@insa-lyon.fr,

<sup>2</sup>Department of Mechanical Engineering, University of Engineering & Technology  
Lahore, Pakistan

Email: engr.ahmad@uet.edu.pk

<sup>3</sup>LFASME, Departamento de Ingeniería Mecánica, Universidad de Santiago de Chile  
Santiago, Chile

Email: dennis.siginer@usach.cl

## ABSTRACT

*A comprehensive study of the rheological characterisation of the aqueous solutions of PEO (Polyethylene Oxide) with molecular mass of  $4 \times 10^6$ ,  $5 \times 10^6$  and  $8 \times 10^6$  g/mol respectively named (4miDA), (5miDA) and (8miDA) was conducted. A large batch of samples of 4miDA PEO with concentrations varying from 0.1% to 3% representing the range of dilute solutions to very high viscous hydrated gels, were tested. Steady state shear flow and oscillatory measurements are reported. Cross, Carreau and Carreau-Yasuda models were used to describe the shear-thinning behaviour within the shear rate range ( $0.001 \leq \dot{\gamma} \leq 3000 \text{ s}^{-1}$ ). Experimental findings were validated with published results under the same operating conditions within specified shear rate ranges ( $0.1 \leq \dot{\gamma} \leq 100 \text{ s}^{-1}$ ). We find that the behaviour of PEO under shear is highly dependent on the rheometer, material and operating procedures. Oscillatory measurements were carried out to determine the complex properties of the PEO solutions in the frequency  $\omega$  and strain amplitude  $\gamma$  ranges of ( $0.01 \leq \omega \leq 100 \text{ rad/s}$ ) and ( $0.01 \leq \gamma \leq 1000 \%$ ), respectively. Higher magnitudes of dynamic moduli ( $G'$  &  $G''$ ), zero ( $\eta_0$ ) and infinite ( $\eta_\infty$ ) shear rate viscosities, resonant frequencies ( $\omega_{res}$ ), linear viscoelastic regions (LVER), and higher relaxation time constants ( $\lambda$ ) were observed with increasing concentration and molecular weight. The rheological response of the PEO polymeric solutions was further clarified via Lissajous curves. The aim of this work is to characterize the behaviour of the 4miDa PEO prior to its use in an experimental investigation of the secondary flows of viscoelastic fluids in non-circular channels.*

**Keywords:** PEO polymer; Rheological characterisation; Shear testing; Dynamic testing.

## 1. INTRODUCTION

The existence of secondary flows in isothermal as well as non-isothermal laminar flow of non-linear viscoelastic fluids in tubes of arbitrary cross-section is well established. The transversal flow field stems from both the non-linear constitutive structure of the viscoelastic fluid and the non-circular geometry of the tube and is driven by the unbalanced second normal stress

---

<sup>1</sup> Dr. M'hamed Boutaous : mhamed.boutaous@insa-lyon.fr,

differences in the cross-section, Siginer [1,2] and Li et al. [3]. The mathematically necessary and sufficient conditions for the existence of a secondary field are elucidated in Siginer [1,2]. The transversal field carries momentum towards the walls. Although, it is two orders of magnitude weaker than the longitudinal flow, it contributes a non-negligible amount to the overall energy loss as particles follow helical paths in the longitudinal direction on cylinders with non-circular directrices as opposed to the straight-line paths in circular tubes. The more elastic the fluid the shorter the generatrix of each cylinder that is the more compressed each helix becomes.

Optical measurement techniques are preferred for quantitative measurements of the transverse velocities in laminar flow of viscoelastic fluids. Special optical characteristics of the working viscoelastic fluid are required for good and reliable measurements. Especially the good optical transparency of PEO to visible light is a desirable property for accurate and repeatable optical measurements. PEO is a high molecular weight polymer with chemical structure of  $[\text{OCH}_2\text{CH}_2]_n$ . The degree of polymerization is represented by  $n$ , which ranges between 2000 and 100,000, Xie and Hartnett [4]. PEO has an extensive range of applications including melt extruded films, oral solid drug delivery technologies, hot melt extrusion and biomedical devices, Upadhye and Rajabi-Siahboomi [5]. It is used as a thickening or thinning agent with solvents including water, as a drag reducing polymer in many industries and as a rheology modifier for organic solvent systems, Braun and Rosen [6]. Hydrophilicity of PEO makes it a good candidate for use as humidity sensors, Sajid et al. [7]. (PEO) belongs to the class of non-linear polymeric solutions the non-linear constitution of which coupled with non-circular cross-sectional geometry, generates secondary flows which in turn significantly enhances heat transfer through the wall, Siginer and Letelier [8], Letelier et al. [9], Siginer et al. [10, 11] and Musil and Zatloukal [12]. Polymeric additives added to the working fluid in the Rayleigh-Bénard convection modify the flow structure and the heat transfer rates in the cell both in laminar, Zheng et al. [13,14] and turbulent flows,

Ahlers and Nikolaenko [15] and Cai et al. [16]. Also, the shear-thinning capability of this type of fluid can contribute substantially to the mixing efficiency enhancement.

Low shear rate shear-thickening of PEO has been investigated in the literature. Vrahopoulou and McHugh [17] conducted a study of PEO in various solvents and found PEO/ethanol solution never shows shear thickening and no plateau is attained until the shear rate of  $3000 \text{ s}^{-1}$ . Georgelos and Torkelson [18] reported shear thickening behaviour of dilute aqueous PEO solution at high shear rates  $\dot{\gamma} > 10^4 \text{ s}^{-1}$  and found the shear thickening behaviour is dependent on the age of the solution. There exists a lot of discussion about shear-thickening around critical concentration and critical shear rate, but the phenomenon has not been investigated in-depth and settled on firm grounds, Liu et al. [19].

To the best of our knowledge, the literature on the rheology of the PEO is rather thin in the all-important lower shear rate region ( $\dot{\gamma} < 1 \text{ s}^{-1}$ ), which is the dominant region in very low Reynolds number flows. We note, besides its fundamental importance, the determination of the behaviour of PEO in the low shear rate region is very relevant to several industrial processes, the extrusion and injection moulding processes among them Liu et al. [20]. The experimental work of Ebagninin et al. [21] and Bahlouli et al. [22] to determine critical concentrations and the effect of temperature on the behaviour of PEO (1miDA) is noted, but there is a lot left to understand the full spectrum of the behaviour of PEO. For example, at higher concentrations, linking weighted relaxation spectrum to the frequency sweep measurements is an important area to be explored. Starting from this perspective, the present study offers a wide range of shear and dynamic measurements about the behaviour of the aqueous PEO.

## 2. MATERIALS AND METHODS

### 2.1 Solution Preparation Protocols

The tested polymer PEO was manufactured by *Polysciences Inc. Europe GmbH*. Three different molecular weights, (4, 5, and 8miDA) as specified by the manufacturer, are tested. 100 ml of each concentration (0.1%, 0.5%, 1%, 1.7%) of PEO 4miDa solution was prepared in distilled water. Initially the beaker contained half volume of the solvent (50 ml). An appropriate amount (0.1g, 0.5g, 1g, 1.7g ± 0.001 g) of fine PEO powder was gently spread uniformly over the solvent with simultaneous stirring to avoid agglomeration of the solute particles. Later the remaining half of the solvent was added to reach the proper concentration.

The mass concentration of the polymer solution is calculated using the following equation

$$C(\%) = \frac{m_{polymer}}{m_{solution}} \times 100 \quad (1)$$

where  $m_{polymer}$  and  $m_{solution}$  are the masses of the polymer powder and final solution, respectively. The unstirred non-homogeneous solution was kept for 60 minutes for proper hydration and swelling after homogenization followed by gentle stirring with a magnetic stirrer (*heidolph instruments GmbH-Teflon coated stirrer*) at fixed temperature of 25 °C at the RPM shown in Table 1.

The homogeneity and uniformity of the solution was achieved as best as possible avoiding solute particle agglomeration (clump formation), flocculation and bubble formation during dispersion and dissolution. Uniformly homogenized solutions require avoiding strong interfacial interaction between polymer chains. Dispersion of PEO molecules in water molecules and diffusion of water molecules in PEO molecules affect the dissolution rate. The size of the PEO molecules can also affect the proper dissolution, Kong et al [23].

Table 1 shows the corresponding RPM and time for continuous stirring with a magnetic stirrer for different concentrations

## 2.2 Rheological Measurement Methods

All rheological measurements were done using an *Anton Paar-MCR 702* stress-controlled Rheometer, equipped with a cone-plate geometry (Cone-plate with diameter and truncation angle 50mm-1° & 25mm-3°), with operating temperatures 20, 23, 25 ± 0.1 °C depending on requirement. The distance between the measuring cone and the bottom plate was carefully adjusted to 0.103mm as suggested by the manufacturer. Errors in the gap adjustment may influence the accuracy of the measurements. Stability characteristics of aqueous PEO suggest that PEO is very sensitive to shear agitation, Braun and Rosen [6]. Care was taken in handling the samples in that regard. For example, Glass syringes (10mL) were used to load the samples from the beaker onto the working table of the Rheometer. Since PEO solutions were found to have memory effects, a pre-shear of 10 s<sup>-1</sup> for 2 mins was applied followed by a recovery with the same time period following Ebagninin et al. [21]. Temperature was kept constant throughout the experiment by means of closed convection chambers the rheometer is equipped with, and a temperature tolerance of ± 0.1 °C throughout the whole experiment was observed.

## 3. RESULTS

All experiments were conducted in the CSR mode (Controlled shear rate mode) settings of the rheometer. The shear rate and the RPM of the spindle (cone) are taken as pre-set parameters and shear stress and torque are to be calculated.

### 3.1 Flow Curve

The correct explanation of the unusual behaviour of this fluid, particularly at low shear rates, requires the proper identification and verification of the role of the operating conditions, especially regarding the repeatability of the measurements and the stability of the measuring conditions. The torque and the rate of applied shear, as well as the elapsed time to reach the steady state conditions are important.

### 3.1.1 Validation of Experimental Results with Literature

Figure 1 shows the comparison of the flow curves of 4miDa PEO with those in the literature. Two different concentrations 0.5% (dilute solution) and 1.7 % (higher concentration solution) were prepared and tested with CP-50-1° at  $23 \pm 0.1^\circ\text{C}$  and CP-25-3° at  $25 \pm 0.1^\circ\text{C}$ , to match the exact similar operating conditions used by Casanellas et al. [24] and Mirsepassi and Rankin [25], respectively.

The resulting flow curves show typical shear-thinning/pseudo-plastic behaviour characterized by decreasing viscosity with increasing shear rate. The shear-thinning character of PEO comes, among other reasons, from the disentanglement of the polymeric chains which behave as worm-like micelles facilitating the flow, Ebagninin et al. [21]. Our experimental data is confirmed by the data of Casanellas et al. [24] and Mirsepassi and Rankin [25] allowing for the experimental uncertainty and scatter. The slight differences with the data of Mirsepassi and Rankin [26] in the lower shear rate region may be due to differences in the protocol of sample preparation and the origin of the polymer as the suppliers are not the same. Mean absolute percentage difference (MAPE) of 1.6 % and 4.3 % was observed with the experiments of Casanellas et al. [24] and Mirsepassi and Rankin [25], respectively.

### 3.1.2 Validation with Viscosity Models and Repeatability

1% aqueous solution of 4miDa PEO was prepared and tested at CP-50 -1° at  $20 \pm 0.1^\circ\text{C}$  to investigate the effect of the shear rate ( $\dot{\gamma}$ ) on the apparent viscosity ( $\eta$ ). A large range of shear rate up to six decades ( $0.001 < \dot{\gamma} < 3000 \text{ s}^{-1}$ ) starting from low to high shear rates was applied to the sample with steady state achieved only when the viscosity becomes constant with a deviation of at most 0.5%. The experiment was run five consecutive times to ensure repeatability and results are shown on Figure 2.

The increasing viscosity in the lower shear rate region ( $0.001 < \dot{\gamma} < 0.011 \text{ s}^{-1}$ ) indicates that the sample is thickening. When the critical value of the shear rate ( $\dot{\gamma}_{cr} = 0.011 \text{ s}^{-1}$ ) is exceeded the

sample starts thinning rather rapidly. The physical reasoning behind this is attributed to the stretching of the flexible polymer chains in the solution. In the low shear rate region, the stretching of the intermingled chains tends to form stationary aggregates before agitation. The chains continue to stretch until the critical value of shear rate is reached ( $\dot{\gamma}_{cr} = 0.011 \text{ s}^{-1}$ ). The chains start losing their bonding within the aggregates and the polymeric chains gradually align themselves in the direction of shear after the critical value is exceeded.

Thus, the solution starts to thin. This phenomenon, even though not studied in-depth, is nevertheless highlighted by some authors who observed a shear-thickening behaviour for polyethylene oxide in water and ethanol solutions, Vrahopoulou and McHugh [17] and Georgelos and Torkelson [18], respectively. A similar trend was found with dilute poly (diallyl dimethyl ammonium chloride) solutions, Liu et al. [19], and discussed by Benchabane and Bekkour [26]. More details concerning this phenomenon will be provided later in this paper. At higher shear rates all PEO chains are disentangled and aligned with the shear direction. Thus, the sample becomes highly shear-thinning. To make sure that repeatability of the viscosity results is not a concern, a tolerance band with lower and upper limits of viscosity values was plotted, and the maximum variation of 11.7 % at shear rate of  $\dot{\gamma} = 100 \text{ s}^{-1}$  and minimum variation of 1.7 at  $\dot{\gamma} = 1000 \text{ s}^{-1}$  was found.

Figure 3 shows the correlation of experimental findings using, Cross, Carreau and Carreau-Yasuda models (see Table 3). All three models represent the experimental data well especially at the higher shear rates. The particular behaviour of the PEO solutions at very low shear rates will be discussed later in the paper. The representation of the data is slightly less accurate in the lower shear rate region, but the overall fit to the data within the shear rate range of  $(0.0750 < \dot{\gamma}$

$< 3000 \text{ s}^{-1}$ ) is quite good. All parameters are given in Table 3.. The critical shear rate  $\dot{\gamma}_{cr}$  marks the onset of shear-thinning and yields the relaxation time ( $\dot{\gamma}_{cr}=1/\lambda$ ).

The numerical values of the parameters of the Cross, Carreau and Carreau-Yasuda models are obtained through fitting to the experimental data. The  $R^2$  value of Carreau and Carreau-Yasuda models shows better fitting of the data as compared to Cross model. Model fitting of experimental data is not accurate in the lower shear rate region ( $0.001 \leq \dot{\gamma} \leq 0.1 \text{ s}^{-1}$ ), Fig. 3, where special molecular phenomena occur like shear-thickening. Ma et al. [27] or Tanaka et al. [28] studied these issues. The accuracy of the viscosity estimates of the models used is only as good as the accuracy of the data fitting.

### *3.1.3 Steady State Achievement Evidence: By Experimental datasets*

Low torque measurements are quite challenging in rotational rheometers. The RPM of the spindle sets the shear rate. Any unsteadiness in the input torque value leads to uncertainty in the shear viscosity measurement. To verify the torque steadiness during data acquisition, several consecutive measurements are taken at the same torque value. The operating conditions of the experiments were exactly the same as in the above section. Every measurement was repeated three times with 60 s imposed to reach equilibrium up to the shear rate  $\dot{\gamma} = 0.1 \text{ s}^{-1}$  and thereafter 30s up to the shear rate of  $3000 \text{ s}^{-1}$ . The shear-thinning flow pattern and continuously rising steady torque curve with fluctuations in the data points could be seen in Figure 4.

Same data (viscosity, torque and shear rate) are plotted against time in Figure 5. The torque starting and ending curves are generated by connecting the torque measurement points in the beginning and at the end, respectively. Thus, clearly torque values stay almost the same at the start and at the end signalling steady torque input. The torque sensitivity envelope can be developed from these torque input curves.

### 3.2 Growth of Transient Viscosity Envelope

A series of measurement artefacts, for example, specification of instrument, instrument and sample inertia, drying of the sample, structural damage of the sample could contribute to the misinterpretation of the viscoelastic responses, Ewoldt et al. [29]. None of the data points should be time affected. The impact of time out (time the spindle takes to achieve steady state over one data point), is always significant. Hence, special care must be taken on the interpretation of the steady shear rheometric experiments. In fact, in such experiments, the liquid in the rheometer is maintained at a particular shear rate for some time needed to measure the viscosity and then move on, inducing a time dependence in the viscosity curves, as the fluids. At each shear rate, the fluid stays for different sufficient time to achieve the steady state. At low shear rates, the equilibration of the polymer conformations takes significantly longer time. Its is what we addressed in figure 6, where it is shown clearly, that for high shear rates, the time out proposed automatically by the rheometer is enough to represent the viscosity evolution in concordance with higher chosen values of time out (here 300s and 1000s). but clearly, for shear rates under  $1 \text{ s}^{-1}$ , the response of the fluid depends strongly on the imposed time out.

Flow curves of 4miDa 1% PEO were plotted under similar operating conditions (CP-50-1°  $20 \pm 0.1$  °C), but with variable time to take the data ( $t_{MP}$ ). For all experiments, the sample was pre-sheared 120 s and left to recover 120 s. Then the shear rate  $\dot{\gamma}$  was varied logarithmically in ascending steps in the range ( $0.001 < \dot{\gamma} < 3000 \text{ s}^{-1}$ ). The three cases studied are shown in Figure 6.a. Case-1: when the timeout achieved automatically by the rheometer. In this case, the rheometer took an average time of 5s to generate one measuring point. Case-2: when the timeout was fixed at 1000s to generate each data point. Case-3: the timeout was fixed at 300s. The latter case corresponds to the same operating conditions used in 3.1.2. The flow curve is made up of two distinct regions. Low shear rate region ( $0.001 < \dot{\gamma} < 0.4 \text{ s}^{-1}$ ) where the viscosity

envelope can be identified, and the higher shear rate region ( $0.4 < \dot{\gamma} < 3000 \text{ s}^{-1}$ ) where the data points from all three sets of measurements overlap. A viscosity peak appears in the lower shear rate region. This peak is either part of the realistic material response or it may be due to experimental errors. For example (5s) may not be enough time or (1000 s) may be too much time for one data point. In the former case, there may not have been enough time to observe the movement of the layers of the sample and in the latter case because of the large time interval, evaporation may have made the sample thicker, thus increasing the viscosity. Thus, 300s for a data point seems to be the optimum time interval for observation. Extending the observation time may yield errors due to evaporation and deterioration of the samples.

The viscosity peak is a function of the observation time. Shear-thickening always happens at low shear rates. But the magnitude of the viscosity at the peak changes depending on the observation time. For short observation times like (5s), the steady state is not reached, and the viscosity curves exhibit a decreasing trend before the Newtonian plateau. It is important to allow enough observation time for each data point not too much and not too short. The former may cause evaporation making sample thicker and further causing deterioration in the sample consistency, and the latter may not allow enough time for the sample to adapt to the shearing conditions in the gap.

This observation is confirmed by reverse testing, Figure 6b, starting from very high to very low shear rates. When the time out is large enough (300 s) for each value of the applied shear rate, the steady state is reached leading to a same behaviour in ascending and in descending shear rates testing. In the descending case, when the low shear rates are reached, the polymer chains are already disentangled but the phenomenon of shear thickening before the Newtonian plateau as in the ascending case with initial pre-shear rate. Note that this concordance could not be

achieved, if the measurement in ascending shearing tests starts suddenly without pre-shear rate, as analysed in the following section.

### 3.3 Effect of Starting Shear Rate

Experiments were run with solutions of PEO 4miDa of different concentrations (0.8%, 1% and 2%) at 20 °C with different starting shear rates. In order to analyse the effect of the starting conditions, no pre-shear rate is applied in this case. The starting value of the shear rate strongly affects the behaviour of the fluids of the concentrations studied in the low shear rates zone. For example, in Figure 7a, the flow curves of 0.8%, 1% and 2% 4miDa with three shear rate ranges ( $0.001 < \dot{\gamma} < 1000 \text{ s}^{-1}$ ,  $0.01 < \dot{\gamma} < 1000 \text{ s}^{-1}$  &  $0.03 < \dot{\gamma} < 1000 \text{ s}^{-1}$ ) were plotted. The shear rate was increased logarithmically with timeout at 300s. The first case ( $0.001 < \dot{\gamma} < 1000 \text{ s}^{-1}$ ) displays an initial shear-thinning region with upwards concavity, followed by a Newtonian plateau and then a shear-thinning zone. Such behaviour is not exhibited by the fluid, when subjected to a pre-shear rate in ascending shearing tests, nor in descending case. This peculiar behaviour of PEO could be explained by the alignment and disentanglement of PEO chains in the water solution when sheared at very low shear rates. Since PEO is highly hydrophilic in nature and subject to flocculation, it tends to behave differently under different values of sudden initial shear rates. If the experiment starts from a very low shear rate ( $0.001 \text{ s}^{-1}$ ), the curves always follow the same pattern of *thinning-plateau-thinning pattern*, and never present shear-thickening behaviour, for all the tested concentrations. The disentanglement of the chain starts sooner. Higher starting shear rates, case-2 and case-3 yield similar results with an initial shear-thickening zone up to a critical shear rate followed by continuous shear-thinning until the end of the experiment. The shear-thickening behaviour occurs because the PEO chains at rest are entangled causing resistance to flow (shear-thickening) and as they stretch and unfold under shear and align themselves with the flow direction, the zones with constant viscosity followed by the shear-

thinning region are formed. This *thickening-plateau-thinning* behaviour is of great interest as it is highly likely that it would occur during the flow at varying Reynolds numbers like in the case of secondary flows in non-circular tubes. The mechanism for the shear thickening is still not yet completely elucidated and is under discussion in the literature. Further details concerning this thickening behaviour could be found in Ebagninin et al. [21].

For the three concentrations, we note that for very low starting shear rates, the shear thickening behaviour attenuates and the viscosity curve follows the thinning- plateau- thinning sequence versus shear rate. We posit that at low values of the starting shear rates, the entangled polymeric coils in the solvent do not interact much as they are set in motion very slowly and slowly disentangle not displaying much resistance, thus the initial shear-thinning. On the other hand, a high enough starting shear rate for the coils to interact, leads to an initial shear-thickening region before the Newtonian plateau as in cases 2 and 3. Although all experiments yield similar curves after the Newtonian zone, at lower shear rates, at the start of the experiments, there is some difference in the shear-thickening viscosity region. Interestingly, each experiment yields a different Newtonian viscosity value. In fact, the exact value of torque required to shear the sample in the lower shear rate regions, affects the measured value of viscosity as noted previously. This is valid for all three concentrations (0.8%, 1%, 2%) investigated in this study. Similar shear-thickening behaviour was observed at higher concentrations in the literature confirming our results, Liu et al. [19] and Ebagninin et al. [21].

For the same fluids, the plot of the evolution of shear stress versus shear rate, Fig 7b, shows the non-linear shear stress-strain relationships with various gradients as seen throughout the shear sweep for all the samples highlighted in the flow curve in Fig. 7a. These evolutions are in concordance with those observed [21], except for the very low shear rate starting value. This could make us think of yield stress fluid behavior. But we believe that this is an artefact due to a sudden but weak solicitation, allowing the chains to disentangle, suddenly, but in no way a yield

-stress. Indeed, it has been clearly demonstrated in [21] that PEO is not a yield-stress fluid, and confirmed in our experiment when starting from high to low shear rates, presented previously.

### **3.4 Flow Behaviour of Various Molecular Weight PEOs**

The effect of chemical and morphological structure of PEO on rheological behaviour is investigated in this section. Several PEO with higher molecular weights (4, 5 and 8miDa), and 1% concentration of PEO all at  $20\pm 0.1$  °C were tested to analyse the difference in their flow behaviour. The shear rates were varied logarithmically in descending order within the range ( $3000 > \dot{\gamma} > 0.001$  s<sup>-1</sup>) with 300s of timeout.

At low shear rates, macromolecules are highly entangled. The Newtonian viscosity represented by the first plateau in the viscosity evolution is due to the relative balance between the disruption rate of the /entanglements and the rate of creation of new ones. The disruption rate becomes intensive enough with increasing shear rate leading to the gradual orientation of the macromolecular chains in the direction of the flow, hence causing the decrease in the viscosity and the appearance of the shear-thinning region.

The effect of the molecular weight on the rheology of the PEO is shown in Figure 8 and corresponding parameters for the Carreau-Yasuda model are given in Table 4. One striking feature of Figure 8a is the almost identical shear-thinning curves for the three PEO solutions for which data has been plotted. As expected, in the Newtonian plateau zone, the higher the molecular weight the higher is the value of the viscosity. The longer chains in 8miDa have a higher number of entanglements, which develops more resistance and reduces the ability of the chains to move easily, hence the viscosity becomes higher. Therefore, with increasing shear rates shear thinning becomes more pronounced. Similar observations are presented by Fam et al. [30].

The resulting flow curves show pronounced shear thinning behaviour for higher molecular weights, but 4miDa presents a peculiar behaviour as compared to 5miDa and 8miDa as explained in section 3.1.2. All the PEOs (4,5 & 8miDa) represent two types of flow behaviour. The abnormal behaviour of 4miDa PEO could be attributed to the rate of formation of entanglements, which makes the chains of 4miDa a bit stiffer at the very start, whereas 5miDa and 8miDa do not show the same chain stiffness. In the case of the PEO 4miDa the forming aggregates in the beginning of shearing trigger gradually increasing viscosity at low shearing rates followed by the disruption of the entanglements of the long chains and unravelling of the aggregates at higher shear rates with increasing shear rates. The chain length of a polymer is given by the following expression, Cogswell [31]

$$L = M_w * \left( \frac{L_o}{M_o} \right) \quad (2)$$

where  $L$  is the chain length of the polymer,  $M_w$  is the molecular weight of the polymer and  $L_o$ ,  $M_o$  are the length and molecular mass of the repeat unit, respectively.  $L_o/M_o$  is the same for all PEOs tested. The viscosity of 8miDa PEO is higher at lower shear rates as compared to 4miDa and 5miDa. The shear rate at which shear thinning appears decreases with increasing molecular weight, Ortis et al. [32]. But in the range ( $1 < \dot{\gamma} < 100 \text{ s}^{-1}$ ) all three samples have similar magnitudes of viscosity. Except in the higher shear rate zone ( $100 < \dot{\gamma} < 3000 \text{ s}^{-1}$ ), 8miDa is less viscous than 4 and 5miDa. We observe that PEO 8miDa curve bisects 5miDa and 4miDa flow curves at  $\dot{\gamma} = 1 \text{ s}^{-1}$  and at  $\dot{\gamma} = 100 \text{ s}^{-1}$ , respectively, which means 8miDa has a higher shear thinning index (99.9%) compared to 4miDa and 5miDa.

The log-log representation of the zero-shear viscosity  $\eta_0$  with varying molecular weight of PEO by Cross, Carreau and Carreau-Yasuda models is shown in Figure 9. Here,  $\eta_0$  corresponds to the Newtonian plateau on each figure for the models, and the initial low shear viscosity for the

measurements. Note that the Cross-model over-estimates the zero-shear rate viscosity, Ortiz et al [32]. Zero shear viscosity is an increasing function of the molecular weight of PEO as observed also by Akinalan et al [33]. Higher molecular weight leads to increased hydrodynamic volume and chain entanglement increasing viscosity. Higher molecular weights are the cause of greater pseudo-plasticity that is the shear-dependent change in viscosity. Degree of polymerization that determines the molecular weight of the polymer has significant effect on pseudo-plasticity (shear-thinning). The power law index values in the viscosity models are indicative of the higher shear thinning character of 4miDa compared to 5miDa and 8miDa. Larger values of the parameter  $n$  show more sensitivity of the viscosity to the shear rate. Shear-thinning profile of 4miDa is steeper than 5miDa and 8miDa.

### 3.5 Effect of Concentration

Concentrations (0.1%, 0.5%, 1%, 1.7%, 2% and 3%) of PEO 4miDa are tested under the same operating conditions to investigate the effect of the concentration on the aqueous solutions of PEO 4miDa: CP-50-1<sup>o</sup>, 20±0.1 °C, shear rate ( $3000 > \dot{\gamma} > 0.001s^{-1}$ ) in a descending logarithmic variation with timeout of 300 s. This concentration range covers the testing samples from very dilute solutions to concentrated hydrogels as the volume fraction changes from low to high. The solution structure responds differently for different concentrations as shown in Figure 10.

The lowest concentration, 0.1% shows almost (relative) Newtonian behaviour, very slight change in viscosity over the shear rate range of  $\dot{\gamma}=1s^{-1}$  to  $1000s^{-1}$ . The solution with 0.5% concentration shows two different viscosity curves with different slopes. For these low concentrations of 0.1% and 0.5 % and for shear rates up to the borderline values of  $\dot{\gamma} = 3$  and  $0.1s^{-1}$ , respectively, no reading with an acceptable confidence level could be detected by the sensor because the torque developed by the rheometer is very low. Readings for shear rates less than these critical values are attributed to noise. A vertical shift is observed in the lower shear rate region for these low

concentrations of 0.1% and 0.5% due to the solution progressing to a semi-dilute state from a dilute state. The viscosity of the solution increases with increasing concentration. In dilute polymeric solutions e.g. 0.1% and 0.5%, molecules are well-separated from each other and their individual intrinsic properties (like viscosity) will determine the physical properties of the solutions. Dilute solution transits with increasing concentration to semi-dilute state. At concentrations of 1% and 1.7% molecules and coils of PEO start touching each other, creating more entanglements and making the solution more viscous. The concentration of 4miDa PEO does affect the experimentation time required to achieve equilibrium, especially at lower shear rates. At low concentrations, the measurements at very low shear rates become very difficult to stabilize because the viscosity approaches the viscosity of the solvent. Low shear rate viscosity measurements were eliminated for this reason. For example, the concentration of 0.1% of PEO took a lot of time (1-hr) to become steady at lower shear rates ( $\dot{\gamma} < 1s^{-1}$ ), and we were not successful in getting reliable data even after several trials. The low torque limit hindered the measurement for 0.1%. For 0.5%, there appears a falling curve facing upwards and with different slopes in different shear regions. A similar trend of shear-thinning was observed with 0.5% solution in the experiments of Casanellas et al. [24] and with both 0.5% and 0.1% PEO solutions in the findings of Lim et al. [34]. But for 1 % solution, in the lowest decade of shear, there appears shear-thickening, and then shear-thinning. However, for higher concentrations like 1.7%, Newtonian plateau appears followed by shear-thinning. Enhancement of concentrations causes further chain entanglements and hence increases viscosity. Ultimately, flow resistance tends to decline as the solution concentration decreases.

Clearly, relaxation time ( $\lambda$ ) increases as the shear rate at which shear thinning appears decreases with increasing concentration. Interaction between chains may help to form strings making the

characteristic relaxation time longer as represented for example by the flow curves in Feng and Joseph [35].

Figure 11 shows the variation of the zero-shear rate viscosity of various concentrations of 4miDa PEO. Three different regimes with different slopes exist. A steep slope is observed in between concentrations 0.1-0.8%. The slope in the region between concentrations 0.8-1.7% is less steep followed by an intermediate slope in the third region between concentrations 1.7-3%. The overlap concentration is estimated to 0.6 %.

### **3.6 Deformation Tests (Oscillatory Shear Testing)**

An input signal of stress or strain in the form of a sinusoidal wave is applied to the sample and the response is recorded in the form of strain or stress. Depending on CSS (Constant shear stress) or CSR (Constant shear rate) configurations, the dynamic moduli, complex viscosity, LVER (Linear viscoelastic range), and flow point of the viscoelastic fluid are obtained. The input sine wave triggers the response of the material over a wide range covering conditions from close to rest to very high speed. These tests are either the frequency sweep or the amplitude sweep type if either the frequency or the amplitude of the input wave is varied, respectively. Amplitude sweep test dictates the robustness of the material whereas frequency sweep test is related to the rate at which energy is transferred to the sample. First LVER regions were traced by performing amplitude sweep tests and then frequency sweep tests are conducted to make sure that testing takes place within LVER region and the molecular structure of the sample is not plastically altered. The transition of  $G'$  and  $G''$  is a point above which the solid-like behaviour of the material cannot follow the movement due to high velocity (shear stress) and hence, liquid-like behaviour becomes dominant.

### 3.6.1 Amplitude Sweep Test

The response of the viscoelastic material to increasing strain is monitored at fixed frequency and temperature in amplitude sweep tests. LVER (Linear viscoelastic range), yield point ( $\tau_y$ -point of deviation) or yield stress, and flow point ( $\tau_f$ ) are the important parameters of an amplitude sweep test. The strain was swept logarithmically from 0.01-1000 % in our experiments, keeping frequency constant 1 rad/s. The amplitude plot has two distinct parts. The very low shear strain region  $0.0001 < \gamma < 0.00052$  yields slight non-linearity of loss modulus until  $\gamma=0.0052\%$  after which both moduli (storage modulus  $G'$  & loss modulus  $G''$ ) run in parallel as the strain magnitude increases. This parallel behaviour stops at ( $\gamma =0.375$ ), and storage modulus starts decreasing and intersects the loss modulus curve at ( $\gamma =1.2$ ). The corresponding stress at that point becomes a critical stress. That point also defines yield stress  $\tau_y$  (or yield point) that separates the linear response region from the non-linear response. The transition,  $G' > G''$  happens when the behaviour of the material cannot accommodate the high-speed motion hence, liquid-like behaviour becomes dominant. Region between [ $\gamma=0.00001-0.375$ ] defines the LVE range where the material remains a solid and fluid mixture. The intersection of the two curves determines the flow /cross over point of the sample and corresponding stress is flow stress  $\tau_f$ . The structural response of the PEO samples is well described by storage modulus ( $G'$ ) within LVER, the region between yield and flow points. The higher critical strain value means higher structural strength of the polymeric solution. Thus, it requires more energy (Cohesive energy density  $CE = \frac{1}{2} \times G' \times (\gamma_{critical}^2)$ ) to destabilize the structure, Akinalan and Argin [33]. Loss factor ( $\tan \delta = G''/G'$ ) describes the relationship between dynamic moduli. Solid and liquid like behaviour of PEO is described by  $\tan (\delta) < 1$  and  $\tan (\delta) > 1$ , respectively. The  $\tan (\delta)$  curve presents three regions. There is a linear increase between the strain values ( $0.0001 < \gamma < 0.001$ ) resulting from the readjustments of long chains ( $0.22 \leq \tan (\delta) \leq 0.507$ ) followed by a region of

straight horizontal line parallel to x-axis until strain reaches the value  $\gamma = 0.375$  at which point the phases are almost equal around 0.5. Thereafter the loss factor starts to increase linearly again until the amplitude sweep ends.

#### *3.6.1.1 Variation in Flow Point-Imposed Frequency*

The imposed frequency of the oscillation can change the rheological characteristics of the polymeric solution in amplitude sweep testing. Figure 13 shows how imposed frequency changes the dynamic moduli and loss factor values. The amplitude of shear strain was varied logarithmically in the range 0.01-1000%, with 1% 4miDa samples and imposed frequencies were 1rad/s and 10 rad/s.  $G'$  and  $G''$  remain parallel with increasing shear strain. An increase in both moduli is observed when the frequency is increased from 1 to 10 rad/s with the loss factor decreasing. With increasing frequency, the value of the shear strain at which flow occurs also increases from 104% to 150%. The magnitude of the loss factor decreases with increasing frequency. The latter behaviour was also observed with viscoelastic solutions of collagen, Lim et al. [34]. The corresponding flow stresses are 3.516 Pa. and 7.216 Pa at 1rad/s and 10 rad/s, respectively.

#### *3.6.1.2 Effect of the Solution Concentration on Flow Point*

Three concentrations 0.8%, 1% and 1.7% of 4miDa were tested under the same operating conditions. Results are summarised in Figure 14, where the evolution of  $G'$  and  $G''$  versus shear strain is plotted for a given frequency. An increase in LVER occurs with increasing concentrations delaying the onset of flow. Flow point goes to 150% from 35.5% when concentration is increased to 1.7% from 0.8%. This evolution is not linear. Three regimes of evolution are distinguished on the concentration effect on the zero-shear rate viscosity linked to the molecular organization. Macromolecular structure is made up of a hierarchy of microscopic sub-structures. Shear strain-induced structural variation of pseudoplastic fluids yields an increase in flow stress and phase

angle variation. Increasing the concentration of PEO in the solution, i.e. increasing the local population of polymeric chains, leads to the enlargement of LVER and delays the appearance of nonlinear viscoelastic behaviour in oscillating shear strain.

The flow stress for concentrations of 0.8%, 1% and 1.7% are 0.805Pa, 3.516Pa and 22.98Pa, respectively. Thus, with increasing concentration, minimum stress required to make samples flow increases and vice versa.

### *3.6.2 Frequency Sweep Test*

Frequency sweep test shows long time scale (very slow lower shear rate) response at lower frequency, and short time response (very fast-higher shear rate) at higher frequency. It has been suggested that over the course of the frequency range, the polymer chains go through various phases of change, e.g. from entangled structures to long wormlike micelles, then short worm like micelles finally becoming temporal rod like structures at maximum frequency, Lim et al. [34]. Figure 15 shows the variation of the imposed angular frequency ( $\omega$ ) against storage modulus, loss modulus and complex viscosity ( $\eta^*$ ). The operating conditions during the frequency sweep were: 4miDa 1%, CP-50-10, 20 °C,  $\gamma=1\%$  [strain volume],  $\omega$  decreased logarithmically in the range ( $100 > \omega > 0.01$  rad/s) with equilibrium time set to 300s, parameter to be constant for  $\eta^*$ . Signal instability limits the frequency range to 100 rad/s. Storage modulus and loss modulus both increase whereas complex viscosity decreases with increasing frequency.

The weighted distribution of the relaxation spectrum  $H(\lambda)$  as a function of the relaxation time ( $\lambda$ ) is shown in Figure 16 at a temperature of 20 °C.  $H(\lambda)$  shows the intensity of each component. The identification of the relaxation spectrum is based on fitting the experimental loss and storage moduli by a multimode Maxwell model. A commercial software from Anton Paar Company was used with the corresponding rheometer to obtain the data represented in Figure 16.

Each mode corresponds to a given relaxation time. It converts the results obtained from frequency sweep test ( $G'$  and  $G''$ ) into a series of relaxation times over the entire range of imposed frequency. The weighted continuous relaxation spectrum was derived keeping edge preserving regularization as it gives better estimation at the ends of the spectrum ending up with a negatively skewed normal Gaussian distribution equivalent to molecular mass distribution. The continuous relaxation time spectrum is generated from the transition region between the first Newtonian plateau (zero-shear viscosity) and the linear Ostwald de-Wale power law region. The point separating the first Newtonian plateau and the power law region is around  $\dot{\gamma} \rightarrow 0.1 \text{ s}^{-1}$ , Figure 3. The cross-over frequency is  $0.1 \text{ rad/s}$ , Figure 15. These two points are critical in determining the relaxation time. The unique relaxation time of  $11.2 \text{ s}$  is of the order of magnitude of the inverse of  $0.1 \text{ rad/s}$  or  $0.1 \text{ s}^{-1}$ . The sample has viscous predominance in the lower frequency range up to  $0.1 \text{ rad/s}$  as  $G'' > G'$ . Elastic behaviour predominates in the higher frequency region after resonant frequency ( $\omega_{res} = 0.1 \text{ rad/s}$ ;  $G' = G'' = 0.712 \text{ Pa}$ ). The complex viscosity does not change rapidly in the lower frequency range and starts becoming thinning in the higher frequency region. Viscosity remains almost constant in the lower frequency region because the chains remain entangled and start to align with the flow direction only after reaching a certain value of the imposed frequency. Complex viscosity ( $\eta^*$ ) is converted to an equivalent value of the steady shear viscosity ( $\eta$ ) using the empirical Cox-Merz correlation. The internal macro-molecular structure of PEO has enough time to respond to the imposed deformation. Generally, frequency sweep test shows  $G' > G''$  for most of the experimental range.

The experiments were repeated for higher concentrations and validated by the work of Mirsepassi and Rankin [25], as shown in Figure 17. Mean absolute percentage error (MAPE) of 5.7 % and 2.9% was calculated for storage and loss moduli, respectively.

### 3.6.3 Lissajous Plots

Lissajous plots (Plots of sinusoidal waveform of shear strain against sinusoidal shear stress at a certain imposed frequency) represent the sequence of physical processes happening inside the material triggered by the externally imposed parameters. The variation in Lissajous plots represents the sliding of layers in the flow direction. The plots are representations of the phenomenological interlayer stress-strain variation in aqueous polymer solutions. To explore the stress-strain relationship in the viscoelastic samples tested, the wave forms of shear strains are plotted against shear stress, the Lissajous plots, Figures 18 (a-e). These are cyclic behaviour of viscoelastic materials subjected to rotation in the clockwise direction. Large amplitude oscillations were applied to the samples of 4mDa, 1% aqueous solutions, and Lissajous plots were obtained at different strain amplitudes at imposed frequencies of 1rad/s and 10rad/s to elucidate the microstructure response of macromolecules. There is considerable fluctuation in sinusoidal shear stress values at low strain amplitude of 0.01%, Figure 18-a. The straight line in the plot will represent the response of the purely elastic solid. The linear viscoelastic behaviour is reached with an increase in amplitude to 0.1%, Figure 18-b. The response of the viscoelastic material becomes gradually more and more non-linear if the strain amplitude is further increased gradually from 1% to 1000%. The graph changes from elliptical to rectangular/parallelogram with rounded corners indicating the prominence of the non-linear effects as it happens as well in the amplitude sweep test, Figure 14, especially after the curve cross-over point. This is the reason the shear stress is almost maximum when the strain is zero at higher amplitudes with a phase shift of  $\pi/2$ . The change in the amplitude from medium to higher amplitudes induces the change in the microstructural behaviour of PEO molecules altering it to slipping from sticking. "Sticking" and "slippage" are terms describing the piling of the layers over each other and destruction of the stacking sequence, respectively. The transformation of

Lissajous plots from irregular shapes at very low amplitudes to ellipses at very high amplitudes 1000% is a display of the change of elasticity dominant viscoelastic gels into viscosity dominant viscoelastic solutions.

Similar behaviour is observed between strain amplitudes 1-100% qualitatively. Figures 18(a-e) show how the imposed frequency alters the behaviour of PEO. A further comparison of the response to imposed frequency is presented in Figure 19. Larger area enclosed by the Lissajous plots at higher frequency shows larger magnitudes of storage and loss modulus of the samples. Increasing the imposed frequency shifts the yield point, flow point and ultimately the storage and loss modulus of the sample.

#### **4. CONCLUSION**

A comprehensive study of the rheological characterisation of the aqueous solution of PEO is conducted over six decades of shear rates ( $10^{-3} < \dot{\gamma} < 10^{+3}$ ) s<sup>-1</sup>. The results are compared to and validated using published results from the literature. New insights concerning the rheological behaviour of the PEO solutions in particular at low shear rates are arrived at. An unusual shear thickening of the fluid under certain flowing conditions is highlighted.

The rheological behaviour of PEO is not only dependent on the material's response, but also on the rheometer and operating parameters. The morphological and rheometric parameters addressed in this study include the molecular weight, concentration of the solutions, the polymer chain type, the age of the solution, timeout, measuring point generation, torque stabilization and starting values of the shear rate. The imposed shear leads to molecular reorientation causing thickening/dilatancy or plateau/Newtonian or thinning/pseudoplasticity.

Relaxation time, which depends on concentration, molecular weight, and imposed frequency has been studied in detail. Increasing concentrations tend to move the cross-over frequency in

the lower frequency region, which makes relaxation time longer. The most concentrated solution takes the longest time to relax indicating increased elasticity. Increasing concentration makes the entanglement network increasingly complex. Thus, increasing the relaxation time as it takes more time to release the internal stresses induced in the sample. A similar trend of increasing relaxation times is observed with increasing molecular weights due to the increasing characteristic length of the polymer chains. Lissajous plots representing the transition of the viscoelastic material from linear to non-linear response are presented.

This in-depth and comprehensive characterization of the PEO solutions will help in the experimental investigation of the secondary flows in non-circular ducts. Work in this regard is in progress currently with PEO as the working fluid in ducts of rectangular cross-section.

**Table 1 Mixing protocols for PEO**

Solution Concentration	Magnetic stirrer (RPM)	No. of Hours for stirring
0.1%	150	16
0.5%	200	20
0.8%	250	24
1%	300	24
1.7%	300	96
2%	300	120
3%	300	144

**Table 2 General form of the different viscosity models and related parameters.**

Viscosity Models	General Form	Parameters in Models	
		Model parameters	Common parameters
Cross	$\frac{\eta(\dot{\gamma}) - \eta_{\infty}}{\eta_0 - \eta_{\infty}} = \frac{1}{1 + (\lambda\dot{\gamma})^{(1-n)}}$	$\lambda$ (s): Time constant $n$ (-): Cross exponent	$\eta(\dot{\gamma})$ (Pa-s): Shear dependent viscosity $\eta_0$ (Pa-s): Viscosity at zero shear $\eta_{\infty}$ (Pa-s): Viscosity at very large shear $\dot{\gamma}$ (s <sup>-1</sup> ): Shear Rate
Carreau	$\frac{\eta(\dot{\gamma}) - \eta_{\infty}}{\eta_0 - \eta_{\infty}} = \frac{1}{(1 + (\lambda\dot{\gamma})^2)^{(1-n)/2}}$	$n$ (-): Dimensionless power-law constant $\lambda$ (s): Relaxation time	
Carreau-Yasuda	$\frac{\eta(\dot{\gamma}) - \eta_{\infty}}{\eta_0 - \eta_{\infty}} = \frac{1}{(1 + (\lambda\dot{\gamma})^a)^{\frac{1-n}{a}}}$	$\lambda$ (s): Dimensional time constant / Relaxation time of fluid $a$ : Parameter describing transition region between zero-shear and power law region $n$ : Power Law index	

**Table 3 Regression parameters for various viscosity models for 4miDA PEO 1% aq. Sol.**

	$\eta_0$ (Pa-s)	$\eta_\infty$ (mPa-s)	$n$	$\lambda$ (s)	$\alpha$	$R^2$
Cross	10.786	18.9	0.294	3.33	Not applicable	0.964
Carreau	9.419	4.7	0.2984	4.5		0.957
Carreau-Yasuda	9.336	8.89	0.27	2.3	1.32	0.99

**Table 4 Carreau-Yasuda regression parameters for 4miDa, 5miDa, 8miDa 1% PEO**

	$\eta_0(Pa-s)$	$\eta_\infty(Pa-s)$	$\lambda(s)$	$a(-)$	$n(-)$	$R^2$
4miDa	9.336	8.89e-3	2.3	1.32	0.27	0.99
5miDa	14.23	8.66e-3	3.2	1.02	0.32	0.997
8miDa	29.2	6.48e-3	6.03	0.73	0.34	0.998

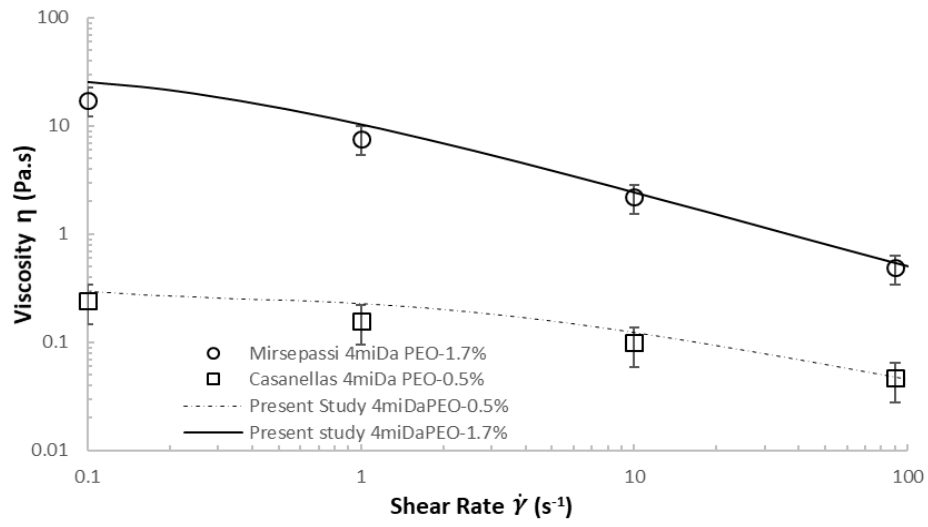


Figure 1 Comparison of available data in the literature with the present study

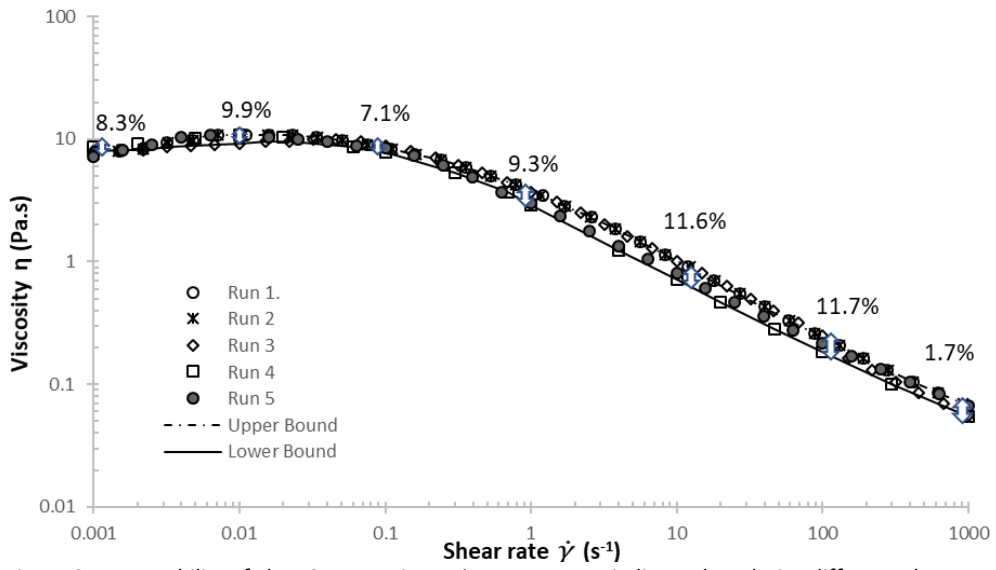


Figure 2: Repeatability of Flow Curve-4miDa 1% - Percentages indicate the relative difference between upper and lower limits.

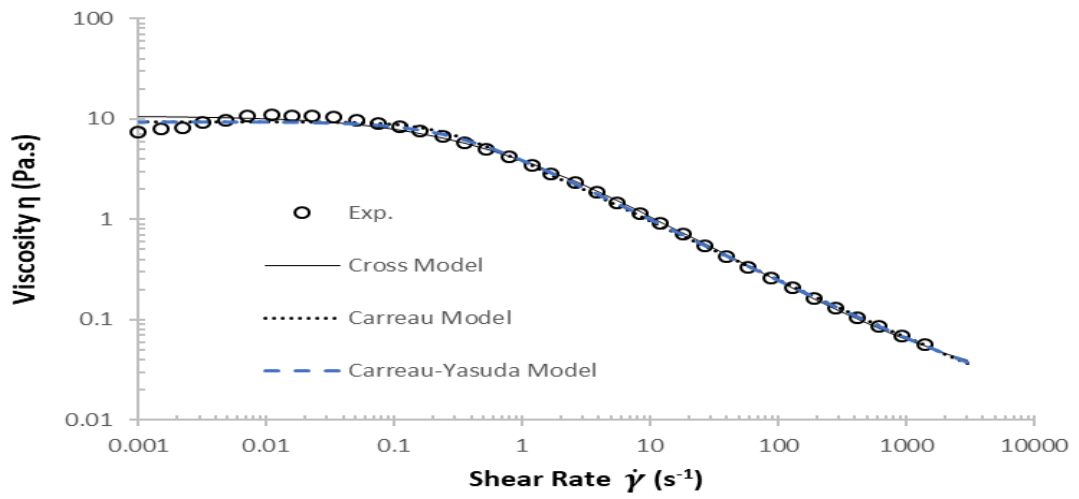


Figure 3 Fitting the experimental data with Cross, Carreau and Carreau-Yasuda models

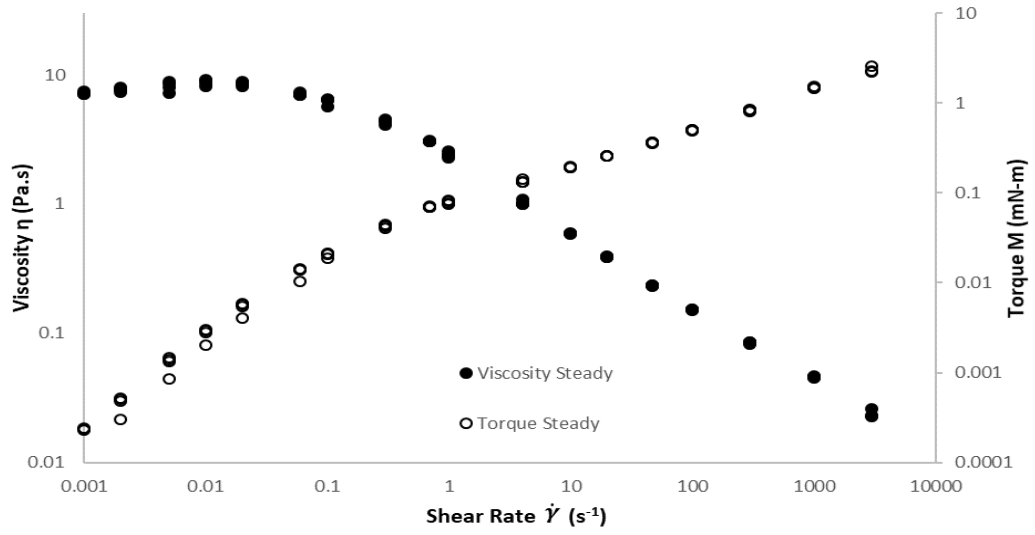


Figure 4 Viscosity and torque evolution curves versus shear rate

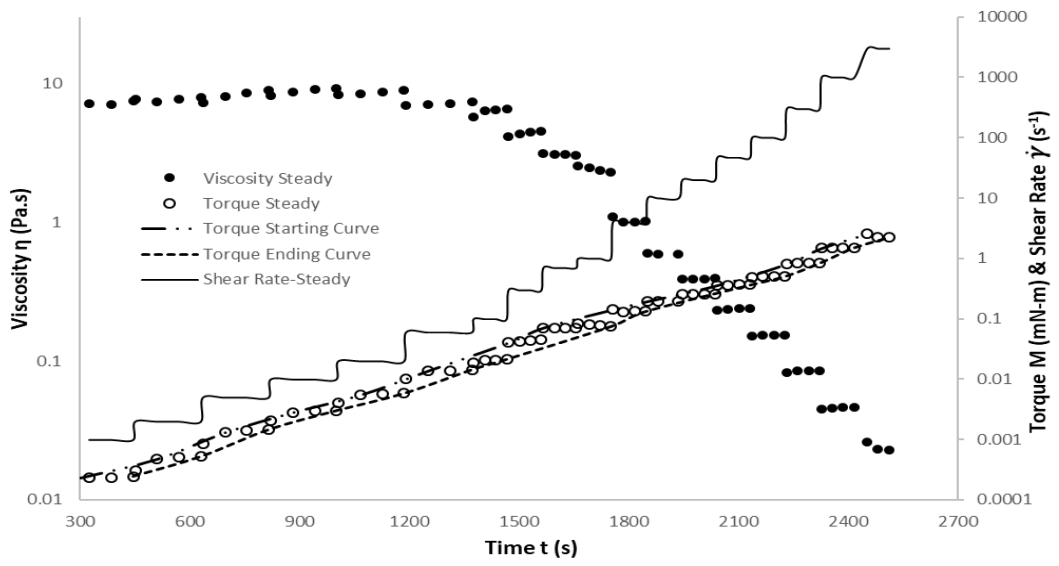


Figure 5 Viscosity and torque evolution curves versus time

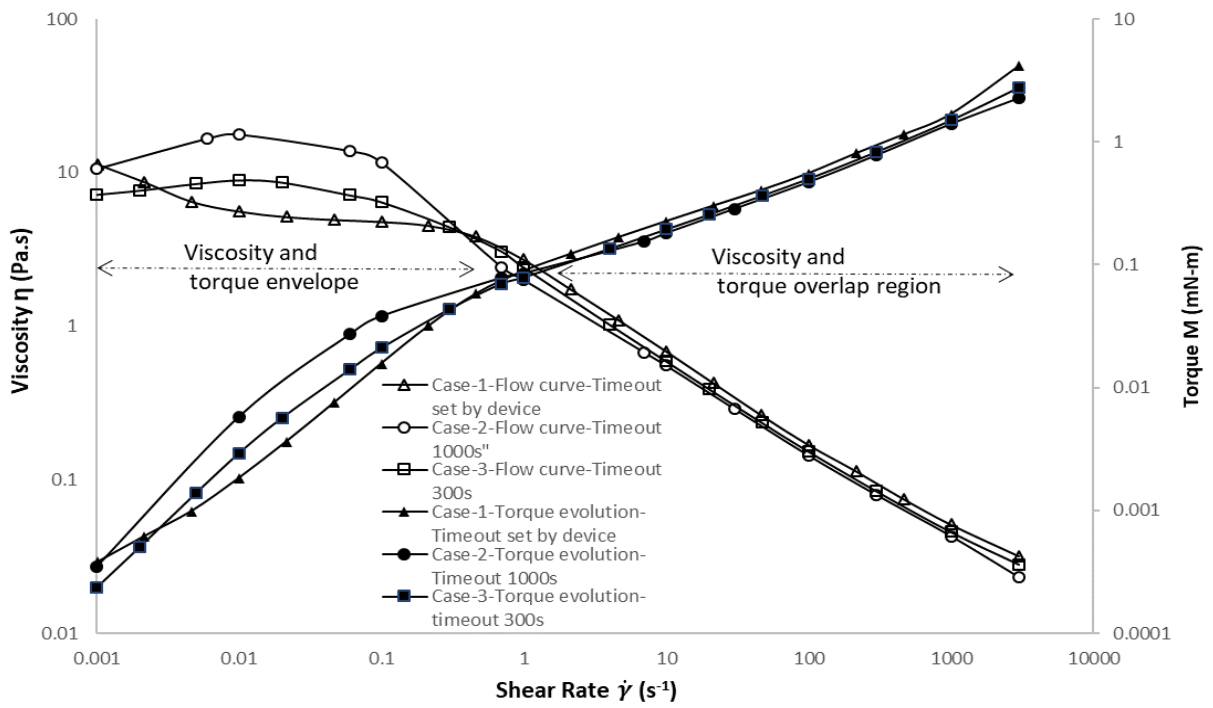


Figure 6a Evolution of transient viscosity and torque envelope

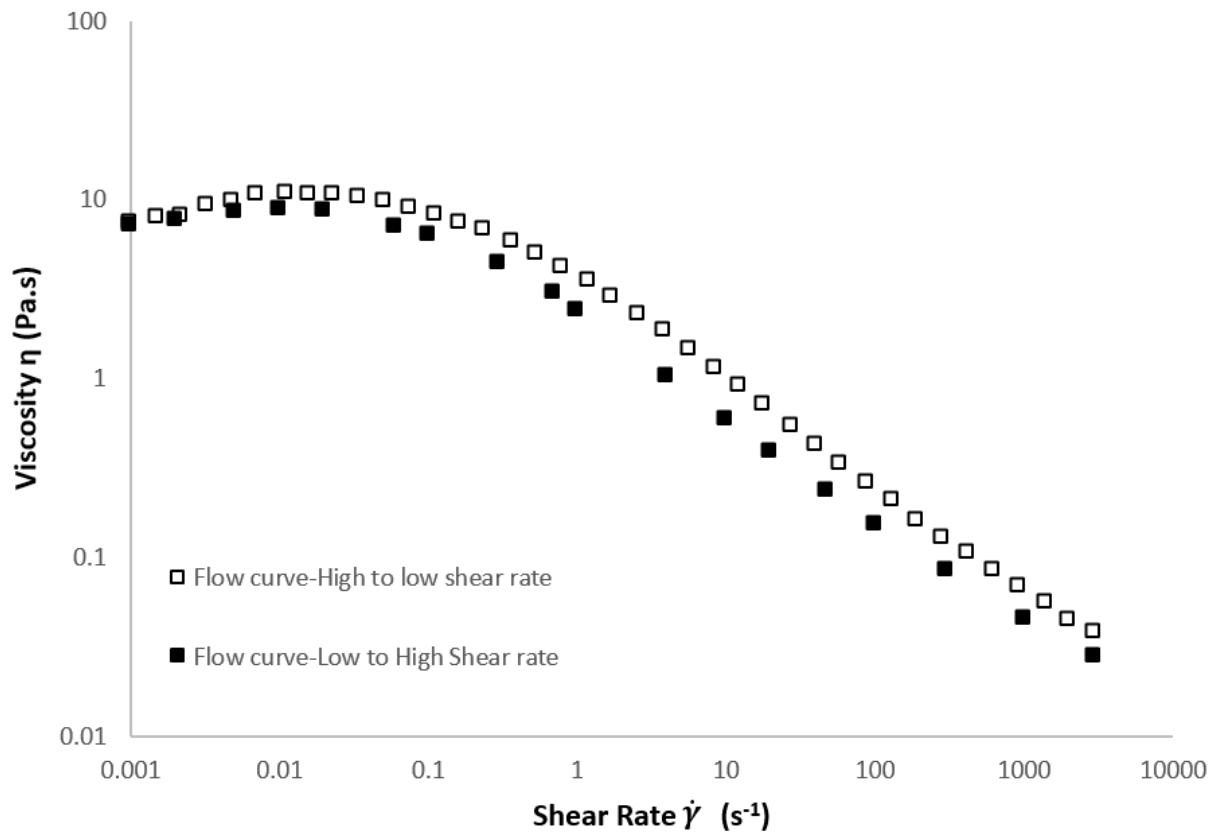


Figure 6b Effect of direction of shear rate: case 3 and 4miDa 1% PEO, 300s time out

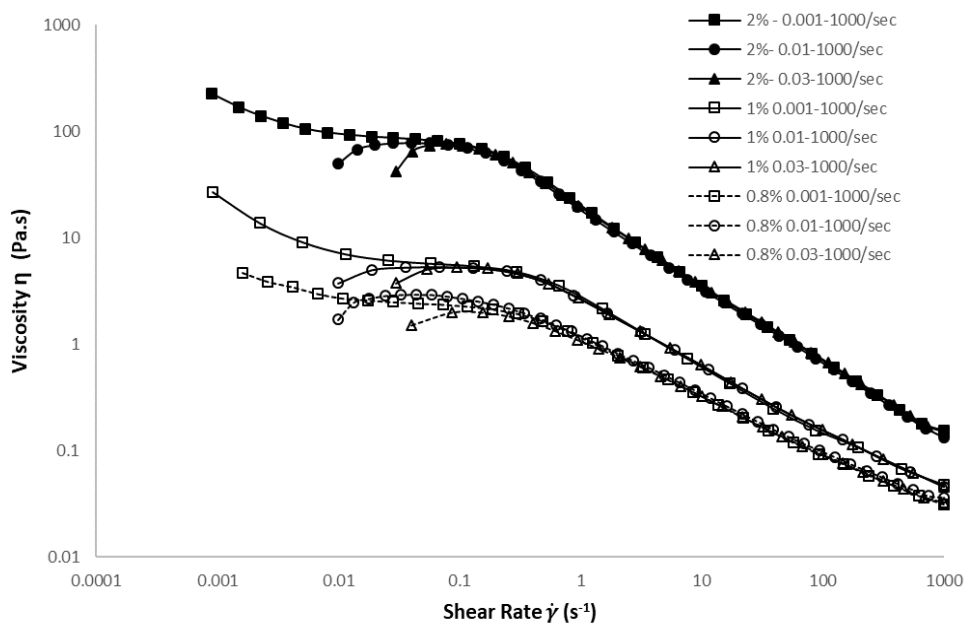


Figure 7a Effect of starting shear rate on 0.8%, 1% and 2% 4miDa PEO Viscosity VS Shear Rate

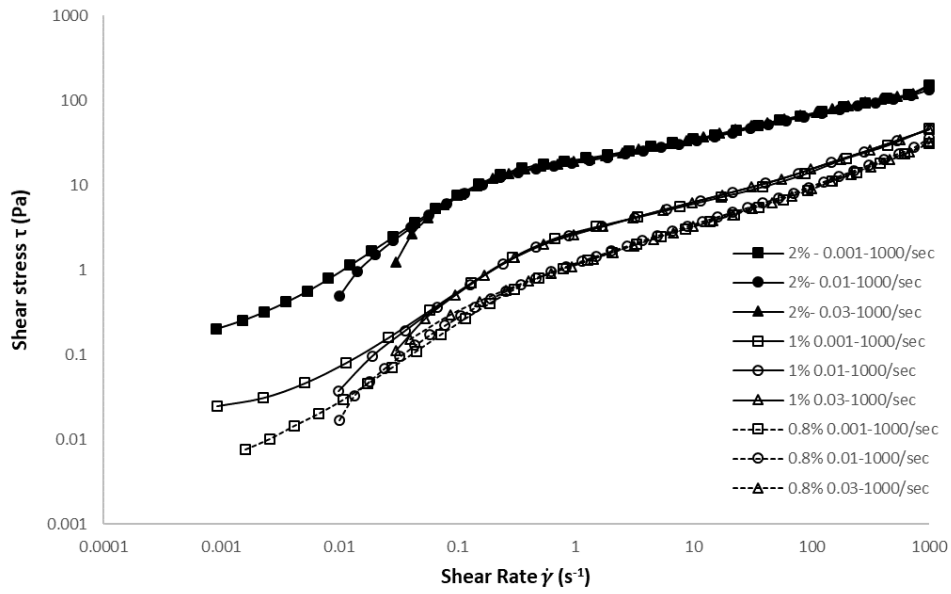


Figure 7b Effect of starting shear rate on 0.8%, 1% and 2% 4miDa PEO-Shear Stress VS Shear Rate

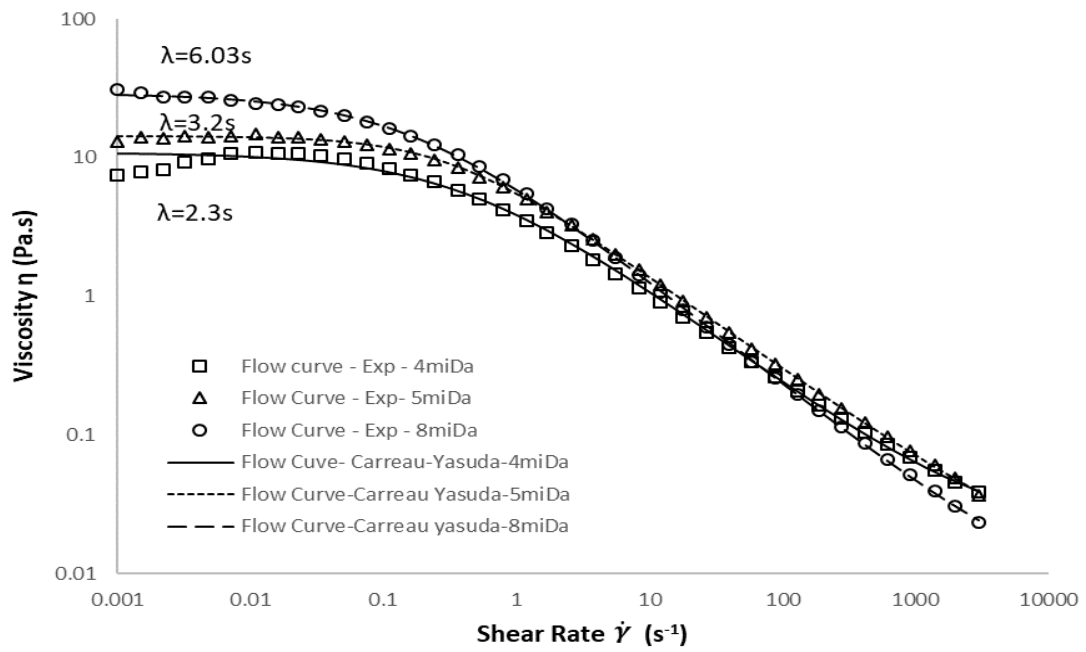


Figure 8 Flow curves for various molecular weight PEOs

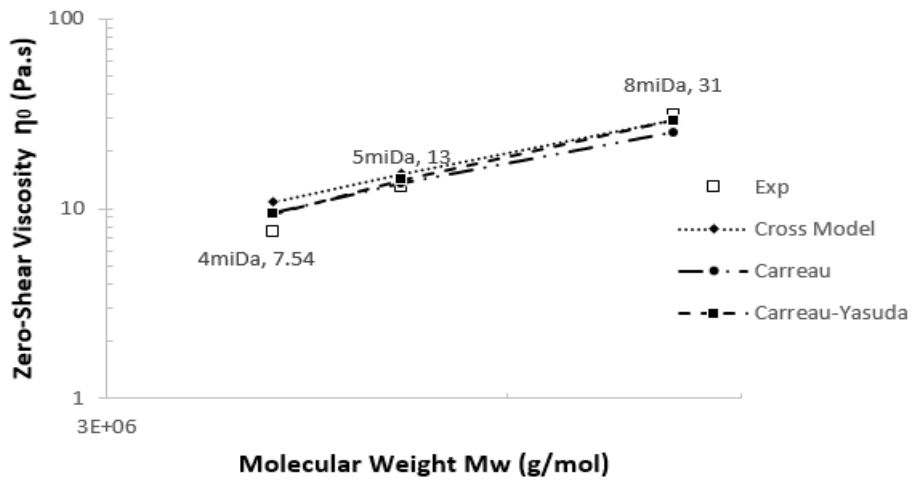


Figure 9 Variation in the zero-shear viscosity with molecular weight of PEO

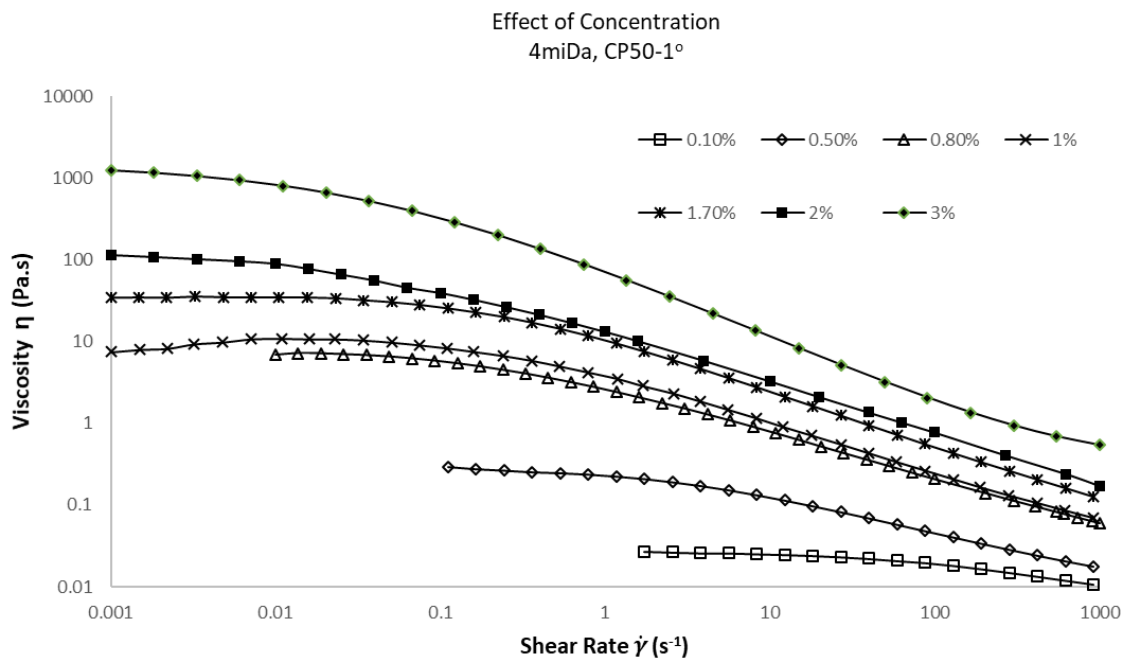


Figure 10 Effect of Concentration-4miDa, CP50 20C

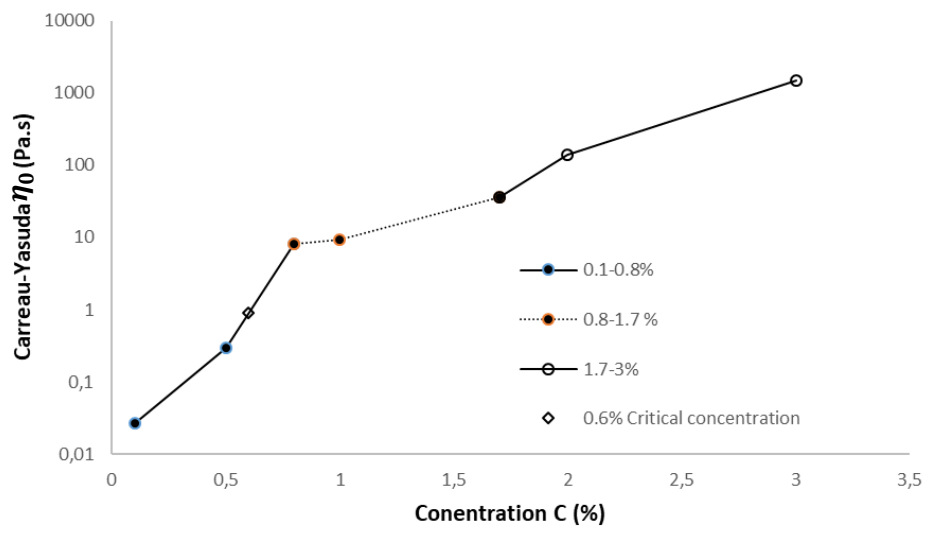


Figure 11 Rise in zero-shear viscosity w.r.t concentration

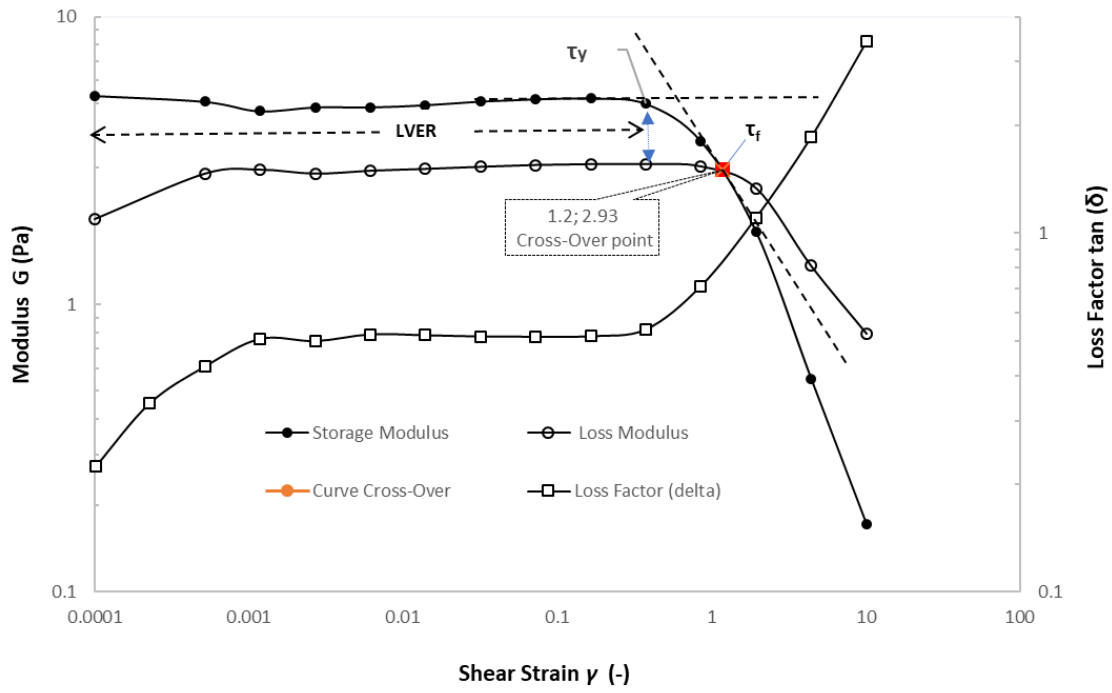


Figure 12 Amplitude sweep test for 4miDa 1% CP50 20 C at imposed frequency 1rad/s

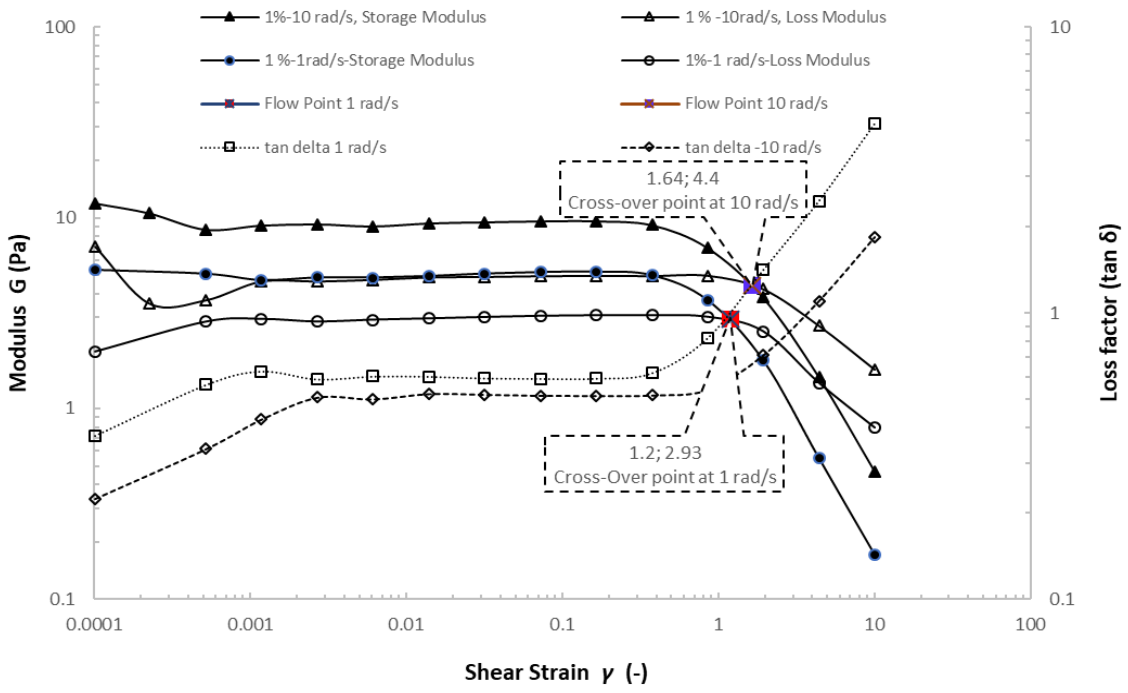


Figure 13 Influence of imposed frequency on flow points

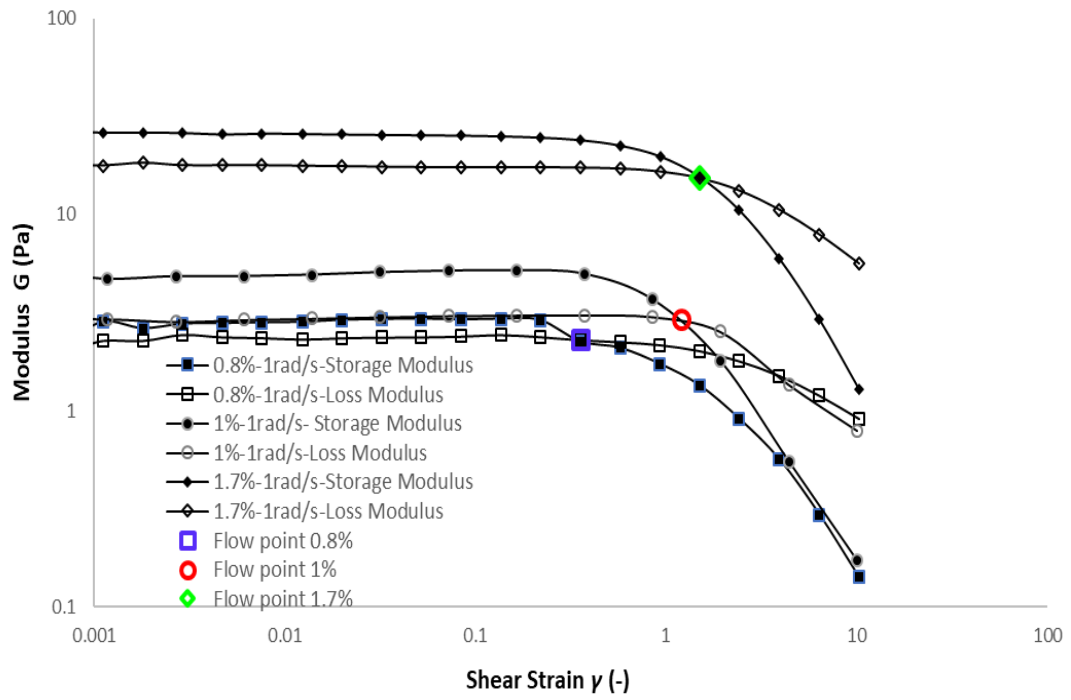


Figure 14 Influence of solution concentration on flow points

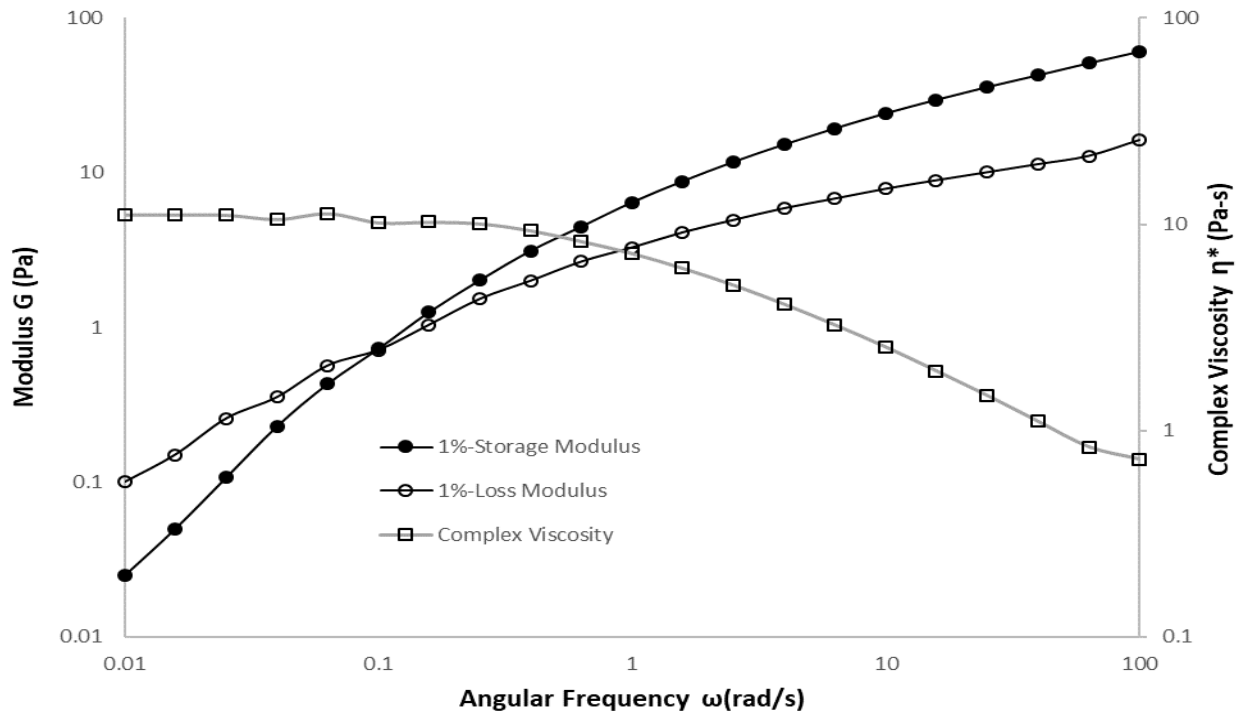


Figure 15 Frequency sweep curve-4miDa 1% CP50 20 °C

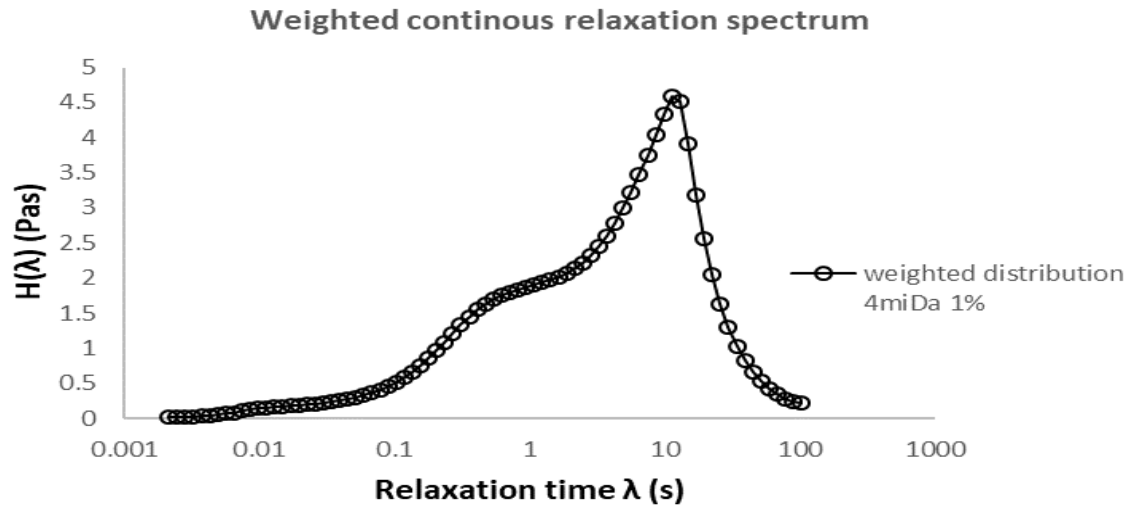


Figure 16 Weighted relaxation spectrum

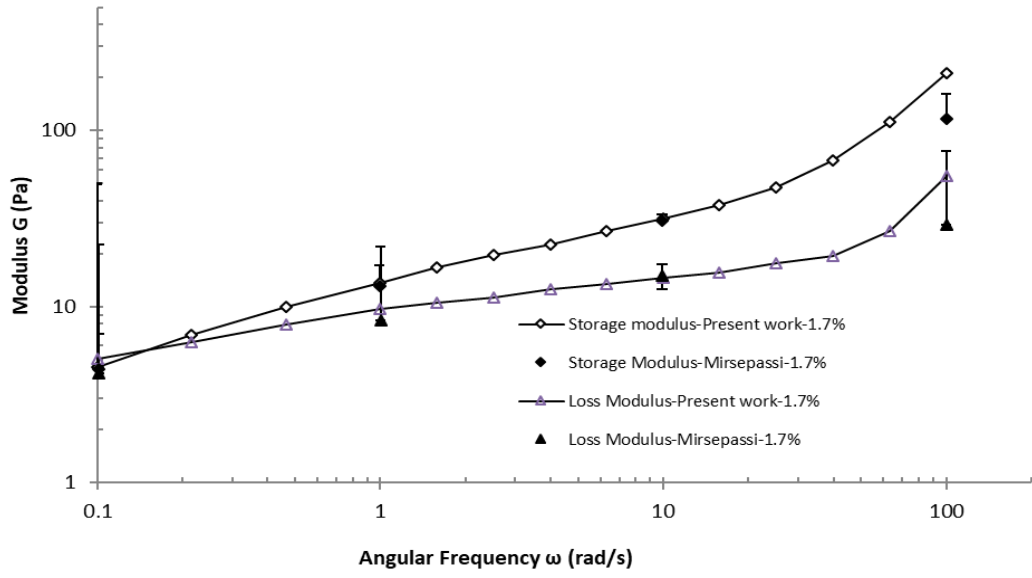


Figure 17 Validation with literature for frequency sweep data

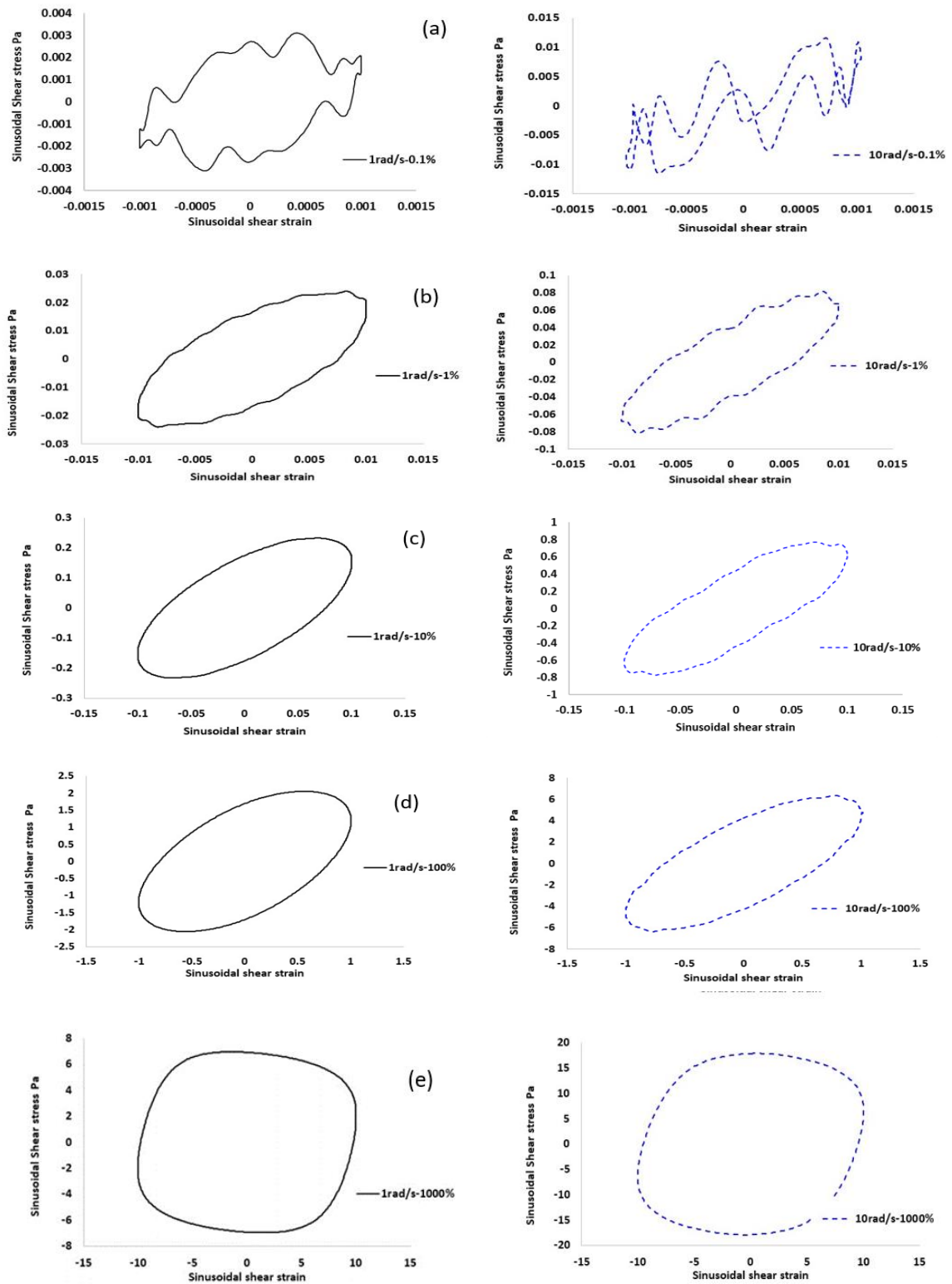


Figure 18 Lissajous plots at different imposed frequency (1 rad/s and 10 rad/s: Solid and dotted line respectively) a-e varying strain from 0.1%-1000%

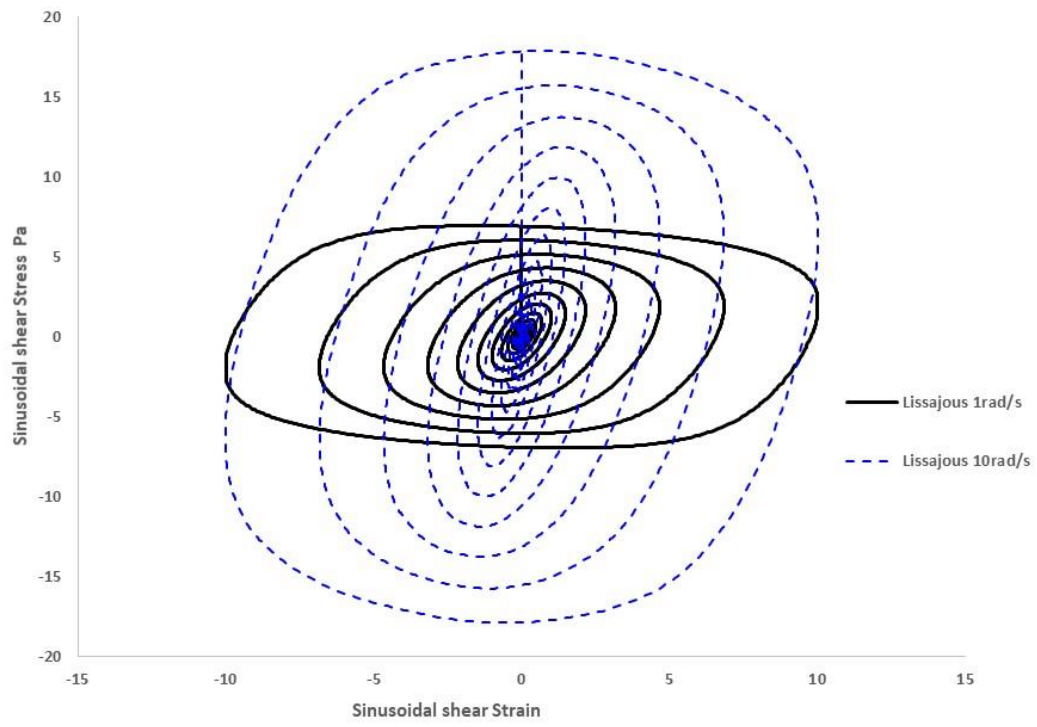


Figure 19 Lissajous plot-CP-50, 20C, 4miDa, 1% Solution,  $\omega=1\text{rad/s}, 10\text{ rad/s}$ ,  $\dot{\gamma}=0.001\text{-}1000\%$

## REFERENCES

- [1] Siginer, D. A., 2011, "Isothermal tube flow of non-linear viscoelastic fluids. Part II: Transversal field", *International Journal of Engineering Science*, 49(6), 443-465.
- [2] Siginer, D. A., 2015, "Developments in the Flow of Complex Fluids in Tubes", Springer International Publishing, ISBN: 978-3-319-02425-7 (hardcover), 978-3-319-02426-4 (eBook), Springer Inc., New York, NY, 2015
- [3] Li, Y. K., Zheng, Z. Y., Zhang, H. N., Li, F. C., Qian, S., Joo, S. W., & Kulagina, L. V., 2017, "Numerical study on secondary flows of viscoelastic fluids in straight ducts: Origin analysis and parametric effects" *Computers & Fluids*, 152, 57-73.
- [4] Xie, C., & Hartnett, J. P., 1992 "Influence of rheology on laminar heat transfer to viscoelastic fluids in a rectangular channel" *Industrial & Engineering Chemistry Research*, 31(3), 727-732.
- [5] Upadhye, S. B., & Rajabi-Siahboomi, A. R., 2013, "Properties and applications of polyethylene oxide and ethylcellulose for tamper resistance and controlled drug delivery" *Melt extrusion*" (pp. 145-158). Springer, New York, NY.
- [6] Braun, D. D., & Rosen, M. R., 2013, "Rheology modifiers handbook: practical use and application", Elsevier.
- [7] Sajid, M., Siddiqui, G. U., Kim, S. W., Na, K. H., Choi, Y. S., & Choi, K. H., 2017, "Thermally modified amorphous polyethylene oxide thin films as highly sensitive linear humidity sensors", *Sensors and Actuators A: Physical*, 265, 102-110.
- [8] Siginer, D. A., & Letelier, M. F., 2006, "Heat transfer in internal flows of non-linear fluids: A review", *ASME International Mechanical Engineering Congress and Exposition* (Vol. 47705, pp. 935-945).
- [9] Letelier, M. F., Siginer, D. A., Barrera, C., González, A., & Boutaous, M. H., 2020, "Forced convection in non-circular tubes with non-linear viscoelastic fluids including viscous dissipation", *International Journal of Thermal Sciences*, 150, 106122.
- [10] Siginer, D. A., Letelier, M. F., Jacobs, P., Aguirre, A., & Boutaous, M., 2020, "Forced convection of elastoviscoplastic fluids in non-circular tubes", *Chemical Engineering Science*, 213, 115318.
- [11] Siginer, D. A., Letelier, M. F., Barrera, C., & González, A., 2019, ".Transversal field and heat transfer in the flow of non-linear viscoelastic fluids in tear-drop shaped tubes including viscous dissipation". *International Journal of Thermal Sciences*, 141, 150-159.
- [12] Musil, J., & Zatloukal, M., 2019, "Historical review of secondary entry flows in polymer melt extrusion", *Polymer Reviews*, 59(2), 338-390.
- [13] Zheng, X., Boutaous, M., Xin, S., Siginer, D.A., Hagani, F. and Knikker, R., 2020, "A new approach to numerical modelling of the viscoelastic Rayleigh-Bénard convection", ASME IMECE, Paper No. IMECE2019-11675, Vol.7, V007T08A028; 7 pages, Salt Lake City, Utah, November 11-14, 2019, published online January 21, 2020.
- [14] Zheng, X., Hagani, F., Boutaous, M., Knikker, R., Shihe, X., and Siginer, D.A., 2022, "Pattern Selection in Rayleigh-Bénard Convection with Non-Linear Viscoelastic Fluids", *Physical Review-Fluids*, 7(2), 023301.

- [15] Ahlers, G., & Nikolaenko, A. 2010, "Effect of a polymer additive on heat transport in turbulent Rayleigh-Bénard convection", *Physical Review Letters*, 104(3), 034503.
- [16] Cai, W., Wei, T., Tang, X., Liu, Y., Li, B., & Li, F., 2019, "The polymer effect on turbulent Rayleigh-Bénard convection based on PIV experiments", *Experimental Thermal and Fluid Science*, 103, 214-221.
- [17] Vrahopoulou, E. P., & McHugh, A. J., 1987, "Shear-thickening and structure formation in polymer solutions", *Journal of Non-Newtonian Fluid Mechanics*, 25(2), 157-175.
- [18] Georgelos, P. N., & Torkelson, J. M., 1988, "The role of solution structure in apparent thickening behavior of dilute ppo/water systems", *Journal of Non-Newtonian Fluid Mechanics*, 27(2), 191-204.
- [19] Liu, W. H., Yu, T. L., & Lin, H. L., 2007, "Shear thickening behavior of dilute poly (diallyl dimethyl ammonium chloride) aqueous solutions", *Polymer*, 48(14), 4152-4165.
- [20] Franck, A., 2004, "Understanding rheology of thermoplastic polymers", TA Instruments, 118, 1-8.
- [21] Ebagninin, K. W., Benchabane, A., & Bekkour, K., 2009, "Rheological characterization of polyethylene oxide solutions of different molecular weights", *Journal of Colloid and Interface Science*, 336(1), 360-367.
- [22] Bahlouli, M. I., Bekkour, K., Benchabane, A., Hemar, Y., & Nemdili, A., 2013, "The effect of temperature on the rheological behavior of polyethylene oxide (PEO) solutions", *Applied Rheology*, 23(1).
- [23] Kong, M., Kang, B. X., & Luo, Y., 2016, "Study of the dissolution of Polyethylene oxide with a high molecular weight in water", *China Pulp & Paper*, 35(12), 20-24.
- [24] Casanellas, L., Alves, M. A., Poole, R. J., Lerouge, S., & Lindner, A., 2016, "The stabilizing effect of shear thinning on the onset of purely elastic instabilities in serpentine microflows", *Soft matter*, 12 (29), 6167-6175.
- [25] Mirsepassi, A., & Rankin, D. D., 2014, "Particle image velocimetry in viscoelastic fluids and particle interaction effects", *Experiments in fluids*, 55(1), 1-7.
- [26] Benchabane, A., & Bekkour, K., 2008, "Rheological properties of carboxymethyl cellulose (CMC) solutions", *Colloid and Polymer Science*, 286(10), 1173-1180.
- [27] Ma, S. X., & Cooper, S. L., 2001, "Shear thickening in aqueous solutions of hydrocarbon end-capped poly (ethylene oxide)", *Macromolecules*, 34(10), 3294-3301.
- [28] Tanaka, F., & Edwards, S. F., 1992, "Viscoelastic properties of physically crosslinked networks. 1. Transient network theory", *Macromolecules*, 25(5), 1516-1523.
- [29] Ewoldt, R. H., Johnston, M. T., & Caretta, L. M., 2015, "Experimental challenges of shear rheology: how to avoid bad data". *Complex Fluids in Biological Systems* (pp. 207-241). Springer, New York, NY.
- [30] Fam, H., Kontopoulou, M., & Bryant, J. T., 2009, "Effect of concentration and molecular weight on the rheology of hyaluronic acid/bovine calf serum solutions". *Biorheology*, 46(1), 31-43.
- [31] Cogswell, F. N., 1981, "Polymer Melt Rheology: A Guide for Industrial Practice", Elsevier.

- [32] Ortiz, M., De Kee, D., & Carreau, P. J., 1994, "Rheology of concentrated poly (ethylene oxide) solutions", *Journal of Rheology*, 38(3), 519-539.
- [33] Akinalan Balik, B., & Argin, S., 2020, "Role of rheology on the formation of Nanofibers from pectin and polyethylene oxide blends", *Journal of Applied Polymer Science*, 137(3), 48294.
- [34] Lim, H., Nam, J., & Shin, S., 2014, "Lateral migration of particles suspended in viscoelastic fluids in a microchannel flow", *Microfluidics and Nanofluidics*, 17(4), 683-692.
- [35] Feng, J., & Joseph, D. D., 1996, "The motion of solid particles suspended in viscoelastic liquids under torsional shear", *Journal of Fluid Mechanics*, 324, 199-222.

## Figure Captions List

- Fig. 1 Comparison of available data in the literature with the present study
- Fig. 2 Repeatability of Flow Curve-4miDa 1% - Percentages indicate the relative difference between upper and lower limits.
- Fig. 3 Fitting the experimental data with Cross, Carreau and Carreau-Yasuda models
- Fig. 4 Viscosity and torque evolution curves versus shear rate
- Fig. 5 Viscosity and torque evolution curves versus time
- Fig. 6a Evolution of transient viscosity and torque envelope
- Fig. 6b Effect of direction of shear rate: case 3 and 4miDa 1% PEO, 300s time out
- Fig. 7a Effect of starting shear rate on 0.8%, 1% and 2% 4miDa PEO Viscosity VS Shear Rate
- Fig. 7b Effect of starting shear rate on 0.8%, 1% and 2% 4miDa PEO-Shear Stress VS Shear Rate
- Fig. 8 Flow curves for various molecular weight PEOs
- Fig. 9 Variation in the zero-shear viscosity with molecular weight of PEO
- Fig. 10 Effect of Concentration-4miDa, CP50 20C
- Fig. 11 Rise in zero-shear viscosity w.r.t concentration
- Fig. 12 Amplitude sweep test for 4miDa 1% CP50 20 C at imposed frequency 1rad/s
- Fig. 13 Influence of imposed frequency on flow points
- Fig. 14 Influence of solution concentration on flow points
- Fig. 15 Frequency sweep curve-4miDa 1% CP50 20 oC
- Fig. 16 Weighted relaxation spectrum
- Fig. 17 Validation with literature for frequency sweep data

Fig. 18 Lissajous plots at different imposed frequency (1 rad/s and 10 rad/s: Solid and dotted line respectively) a-e varying strain from 0.1%-1000%)

Fig. 19 Lissajous plot-CP-50, 20C, 4miDa, 1% Solution,  $\omega=1\text{rad/s}, 10\text{ rad/s}$ ,  $\dot{\gamma}=0.001\text{-}1000\%$

#### Table Caption List

Table 1	Mixing protocols for PEO
Table 2	General form of the different viscosity models and related parameters.
Table 3	Regression parameters for various viscosity models for 4miDA PEO 1% aq. Sol.
Table 4	Carreau-Yasuda regression parameters for 4miDa, 5miDa, 8miDa 1% PEO